

Manuscript Number: GCA-D-17-00380R1

Title: Gallium isotope fractionation during Ga adsorption on calcite and goethite

Article Type: Article

Corresponding Author: Dr. JiuBin Chen, Ph.D

Corresponding Author's Institution: Institute of Geochemistry, CAS

First Author: WEI YUAN

Order of Authors: WEI YUAN; Giuseppe D. Saldi; JiuBin Chen; Marino Vetuschi Zuccolini; JeanLouis Birck; Yujie Liu; Jacques Schott

Abstract: Gallium (Ga) isotopic fractionation during its adsorption on calcite and goethite was investigated at 20 °C as a function of the solution pH, Ga aqueous concentration and speciation, and the solid to solution ratio. In all experiments Ga was found to be enriched in light isotopes at the solid surface with isotope fractionation  $\Delta^{71}\text{Ga}_{\text{solid-solution}}$  up to -1.27 ‰ and -0.89 ‰ for calcite and goethite, respectively. Comparison of Ga isotopic data of this study with predictions for 'closed system' equilibrium and 'Rayleigh fractionation' models indicates that the experimental data are consistent with a 'closed system' equilibrium exchange between the fluid and the solid. The results of this study can be interpreted based on Ga aqueous speciation and the structure of Ga complexes formed at the solid surfaces. For calcite, Ga isotope fractionation is mainly triggered by increased Ga coordination and Ga-O bond length, which vary respectively from 4 and 1.84 Å in  $\text{Ga}(\text{OH})_4^-$  to 6 and 1.94 Å in the  $>\text{Ca}-\text{O}-\text{GaOH}(\text{OH}_2)_4^+$  surface complex. For goethite, despite the formation of Ga hexa-coordinated  $>\text{FeO}(\text{OH})_2$  surface complexes (Ga-O distances of 1.96-1.98 Å) both at acid and alkaline pH, a similar extent of isotope fractionation was found at acid and alkaline pH, suggesting that  $\text{Ga}(\text{OH})_4^-$  is preferentially adsorbed on goethite for all investigated pH conditions. In addition, the observed decrease of Ga isotope fractionation magnitude observed with increasing Ga surface coverage for both calcite and goethite is likely related to the formation of Ga surface polymers and/or hydroxides with reduced Ga-O distances. This first study of Ga isotope fractionation during solid-fluid interactions suggests that the adsorption of Ga by oxides, carbonates or clay minerals could yield significant Ga isotope fractionation between secondary minerals and surficial fluids including seawater. Ga isotopes thus should help to better characterize the surficial biogeochemical cycles of gallium and its geochemical analog aluminum.

1 **Gallium isotope fractionation during Ga adsorption**  
2 **on calcite and goethite**

3 Wei Yuan <sup>a,b</sup>, Giuseppe D. Saldi <sup>c</sup>, JiuBin Chen <sup>a\*</sup>, Marino Vetuschi Zuccolini <sup>d</sup>,  
4 Jean-Louis Birck <sup>e</sup>, Yujie Liu <sup>a</sup> and Jacques Schott <sup>c</sup>

5 <sup>a</sup>*State Key Laboratory of Environmental Geochemistry, Institute of Geochemistry, Chinese*  
6 *Academy of Sciences, Guiyang 550081, China.*

7 <sup>b</sup>*University of Chinese Academy of Sciences, Beijing 100049, China*

8 <sup>c</sup>*Géoscience Environnement Toulouse, CNRS (UMP 5563)-OMP-Université Paul-Sabatier, 14,*  
9 *Avenue Édouard Belin, 31400 Toulouse, France*

10 <sup>d</sup>*Laboratorio di Geochimica at DIPTERIS, Università di Genova, Corso Europa 26, 16132*  
11 *Genova, Italy*

12 <sup>e</sup>*Laboratoire de Géochimie et Cosmochimie, Institute de Physique du Globe de Paris (IPGP),*  
13 *75252 Paris, France*

14 \* *Corresponding author.*

15 *E-mail: [chenjiubin@vip.gyig.ac.cn](mailto:chenjiubin@vip.gyig.ac.cn) Tel.: +86 851 85892669*

16

***Published in *Geochimica et Cosmochimica Acta****  
***Volume 223, 2018, Pages 350-363***  
***<https://doi.org/10.1016/j.gca.2017.12.008>***

17 **ABSTRACT**

18 Gallium (Ga) isotopic fractionation during its adsorption on calcite and goethite  
19 was investigated at 20 °C as a function of the solution pH, Ga aqueous  
20 concentration and speciation, and the solid to solution ratio. In all experiments Ga  
21 was found to be enriched in light isotopes at the solid surface with isotope  
22 fractionation  $\Delta^{71}\text{Ga}_{\text{solid-solution}}$  up to -1.27 ‰ and -0.89 ‰ for calcite and goethite,  
23 respectively. Comparison of Ga isotopic data of this study with predictions for  
24 ‘closed system’ equilibrium and ‘Rayleigh fractionation’ models indicates that the  
25 experimental data are consistent with a ‘closed system’ equilibrium exchange  
26 between the fluid and the solid. The results of this study can be interpreted based on  
27 Ga aqueous speciation and the structure of Ga complexes formed at the solid  
28 surfaces. For calcite, Ga isotope fractionation is mainly triggered by increased Ga  
29 coordination and Ga-O bond length, which vary respectively from 4 and 1.84 Å in  
30  $\text{Ga}(\text{OH})_4^-$  to 6 and 1.94 Å in the  $>\text{Ca-O-GaOH}(\text{OH}_2)_4^+$  surface complex. For  
31 goethite, despite the formation of Ga hexa-coordinated  $>\text{FeOGa}(\text{OH})_2^0$  surface  
32 complexes (Ga-O distances of 1.96-1.98 Å) both at acid and alkaline pH, a similar  
33 extent of isotope fractionation was found at acid and alkaline pH, suggesting that  
34  $\text{Ga}(\text{OH})_4^-$  is preferentially adsorbed on goethite for all investigated pH conditions.  
35 In addition, the observed decrease of Ga isotope fractionation magnitude observed  
36 with increasing Ga surface coverage for both calcite and goethite is likely related to  
37 the formation of Ga surface polymers and/or hydroxides with reduced Ga-O  
38 distances. This first study of Ga isotope fractionation during solid-fluid interactions  
39 suggests that the adsorption of Ga by oxides, carbonates or clay minerals could  
40 yield significant Ga isotope fractionation between secondary minerals and surficial  
41 fluids including seawater. Ga isotopes thus should help to better characterize the  
42 surficial biogeochemical cycles of gallium and its geochemical analog aluminum.

43

44

45

## 46 1. INTRODUCTION

47 Chemical weathering, which is caused by the interaction of water with minerals at  
48 the Earth's surface, plays an important role in continental erosion, soil formation,  
49 plant nutrient release, delivery of dissolved elements to streams and the oceans, and  
50 the control of atmospheric CO<sub>2</sub> concentration and climate (Berner, 1997; Gaillardet  
51 et al., 1999; Galy and France-Lanord, 1999; Hilton et al., 2011; Tipper et al., 2006;  
52 Vance et al., 2009). Among the chemical elements involved in weathering,  
53 aluminum (Al) is of particular interest because it is a major constituent of  
54 rock-forming minerals, especially aluminosilicates such as feldspars, micas and clay  
55 minerals. During weathering processes, Al is sorbed onto and/or incorporated into  
56 inorganic and organic colloids, and its insolubility leads to the formation of  
57 secondary solids such as clays or Al hydroxides (Hydes and Liss, 1977; Hydes,  
58 1979; 1983; Measures and Edmond, 1988; Orians and Bruland, 1988; Pokrovsky  
59 and Schott, 2002; Shiller, 1988; Shiller and Frilot, 1996). Although characterizing  
60 Al weathering chemistry is of importance, this knowledge is still incompletely  
61 understood due to the numerous interactive processes that impact the chemical  
62 behavior of Al. Stable isotope approaches have proven useful for revealing  
63 weathering process and their interactions for other key elements such as calcium  
64 (Gussone et al., 2016; Hindshaw et al., 2011) and magnesium (Opfergelt et al., 2012;  
65 Teng et al., 2010) However, Al has only one naturally-occurring stable isotope (<sup>27</sup>Al)  
66 and thus it is not possible to use Al stable isotope approaches to aid in quantifying  
67 the weathering intensity and the extent of secondary phase precipitation, or to  
68 estimate the respective fluxes of dissolved and particulate Al to the ocean. Thus,  
69 there is value in identifying and developing proxy stable isotope tracers of Al  
70 behavior during weathering to provide additional insights into past and present  
71 alteration processes involving Al that have affected the Earth's surface.

72 Gallium (Ga) has been considered as a potential tool to help decipher Al behavior  
73 during these alteration processes (Goldschmidt, 1954; Burton et al., 1959; Orians  
74 and Bruland, 1988; Shiller, 1988; Shiller and Frilot, 1996). Ga, located just below

75 Al in column IIIA of the periodic table, has two stable isotopes,  $^{69}\text{Ga}$  and  $^{71}\text{Ga}$ , with  
76 abundances of 60.1% and 39.9%, respectively (De Laeter, 1972). Its abundance in  
77 the Earth's crust is approximately 15 ppm (Wedepohl, 1995) and it is found as a  
78 minor constituent in many minerals (Wood and Samson, 2006). Trivalent Ga is the  
79 stable oxidation state at the Earth's surface, and owing to similar ionic radii it  
80 frequently substitutes for  $\text{Al}^{3+}$  and/or  $\text{Fe}^{3+}$  in common rock-forming minerals  
81 (Gottardi et al., 1978). The high charge and small radius of Ga (0.62 Å) rank it, like  
82 Al (0.54 Å), among the “hard” acids according to the classification of Pearson  
83 (1963), thus implying that these cations tend to form solute complexes with hard  
84 donor atoms such as hydroxyls, carboxylates or phenolates.

85 Both  $\text{Al}^{3+}$  and  $\text{Ga}^{3+}$  undergo strong hydrolysis as fluid pH increases with the  
86 formation of hydroxide complexes (successively  $\text{Al,GaOH}^{2+}$ ,  $\text{Al,Ga(OH)}_2^+$ ,  
87  $\text{Al,Ga(OH)}_3^0$  and  $\text{Al,Ga(OH)}_4^-$ ) although the extent of Ga hydrolysis is more marked.  
88 For example, at 25 °C and pH=6, Al aqueous speciation is dominated by  $\text{Al(OH)}_3^0$   
89 and  $\text{Al(OH)}_2^+$  whereas Ga is exclusively present as  $\text{Ga(OH)}_4^-$  (Benézéth et al, 1997;  
90 Tagirov and Schott, 2001). The more effective hydrolysis of aqueous Ga compared  
91 to that of aqueous Al at given temperature and pH has been invoked to account for  
92 both the lower reactivity of Ga (longer residence time) than Al in the oceans, due to  
93 its presence as the more “soluble” gallate complex (Orians and Bruland, 1988) and  
94 the higher mobility of Al in streams as a result of the stronger complexation with  
95 organic matter of the less hydrolyzed Al species (Martell and Hancock, 2013). This  
96 led Shiller and Frilot (1996) to propose the use of dissolved Ga concentration  
97 measurements for estimating the mobilization of Al in watersheds by inorganic or  
98 organic complexation processes for which the weathering regimes are known.

99 Advances over the last decade in multiple-collector inductively coupled  
100 plasma-source mass spectrometry (MC-ICP-MS), combined with the recent  
101 development of chemical purification methods that allow for accurate measurement  
102 of Ga isotopes ratios (Yuan et al., 2016; Zhang et al., 2016; Kato et al., 2017), offer  
103 new possibilities for the use of Ga and its isotopes to decipher the weathering  
104 mechanisms and the behavior of Al in continental surficial waters and in the oceans.

105 Ga isotopes appear to be a new promising tool in this regard, because i) large  
106 variations of  $\delta^{71}\text{Ga}$  (see Eq. (1) for definition of the delta terminology) up to 1.83‰  
107 have already been detected in various standard samples (Yuan et al., 2016; Zhang et  
108 al., 2016; Kato et al., 2017), and ii) the coordination change that Ga undergoes,  
109 from 4 in solution ( $\text{pH} \geq 5$ , Benézéth et al., 1997) to 6 at the surface or in the  
110 crystal structure of oxides and carbonates (Pokrovsky et al., 2004; Persson et al.,  
111 2006), is likely to induce significant isotope fractionation as a result of the increase  
112 of the metal-oxygen bond length (Criss, 1999; Schauble, 2004; Schott et al., 2016).

113 Adsorption on oxides, clays, carbonates, and inorganic and organic colloids is  
114 known to be an important process in the control of trivalent elements like Ga in  
115 surficial environments and their scavenging from natural waters (Pokrovski et al.,  
116 2002; Gaillardet et al., 2003; Pokrovsky et al., 2004, 2006). The structure of the  
117 complexes formed by Ga at the surface of carbonates (calcite, magnesite) and  
118 oxides (birnessite, goethite) has recently been characterized using X-ray Absorption  
119 Spectroscopy (Pokrovsky et al., 2004; Persson et al. 2006). The present study  
120 extends this knowledge to Ga isotope fractionation during Ga adsorption on calcite  
121 and goethite. It is expected that this work will allow identification and quantification  
122 of the physico-chemical parameters controlling Ga isotope behavior in the presence  
123 of Fe hydrous oxides and carbonates, and provide the first constraints on the extent  
124 of Ga isotope fractionation in aquatic environments at the Earth's surface.

## 125 **2. MATERIALS AND METHODS**

### 126 **2.1. Starting Materials**

127 Synthetic calcite and goethite were used for the adsorption experiments. Calcite  
128 powder with sub-micrometer crystal size was obtained by precipitation from  
129 supersaturated solutions of  $(\text{NH}_4)_2\text{CO}_3$  and  $\text{CaCl}_2$  at  $\text{pH} \sim 10$ . The goethite powder  
130 (aggregates of crystals having an average size of 0.1  $\mu\text{m}$ , as determined by laser  
131 diffraction technique) was synthesized in the LEM laboratory (Nancy University,  
132 France) following a procedure described by Cornell and Schwertmann (2004) and  
133 based on the oxidative hydrolysis of  $\text{FeSO}_4$ . Both powders were from the same

134 batches previously characterized by Pokrovsky et al. (2004, 2006) to investigate Ga  
135 and Ge adsorption on calcite and goethite, respectively. Supplementary X-ray  
136 diffraction analyses provided verification of their crystallinity and the absence of  
137 other phases. Trace element analysis of studied solids performed by ICP-MS did not  
138 detect any impurities in amounts  $\geq 0.1$  wt%, and Ga content was below 1 ppm. The  
139 specific surface area of calcite and goethite was  $18.6 \text{ m}^2/\text{g}$  and  $23.2 \text{ m}^2/\text{g}$ ,  
140 respectively, as determined by the B.E.T. nitrogen adsorption technique.

141 For the Ga adsorption experiments, a 1000 ppm  $\text{Ga}^{3+}$  stock solution was prepared  
142 by dissolving Ga (III) nitrate hydrate (Puratronic®, 99.999%, by Alfa Aesar) in  
143 ultrapure water ( $18.2 \text{ M}\Omega\cdot\text{cm}$ ) and adjusting the pH to 1.5 by addition of  $\text{HNO}_3$ .  
144 From this stock solution, other solutions of lower Ga concentrations (1~10 ppm) at  
145 near-neutral pH were prepared. These solutions were freshly made each time before  
146 starting the experimental runs and added immediately to calcite and goethite  
147 suspensions, in order to prevent any possible precipitation of Ga oxyhydroxide  
148 before use.

149 All labware (Teflon vials, pipette tips and storage bottles etc.) was carefully  
150 cleaned in an ultra-clean room following an established procedure that entails the  
151 use of EXTRANS solution, a mixture of concentrated HCl and  $\text{HNO}_3$ , HF, and 1 M  
152 HCl and repeated washing with ultrapure water.

## 153 **2.2 Adsorption experiments**

154 The adsorption experiments were carried out at the GET laboratory in Toulouse,  
155 France. Both series of experiments on calcite and goethite were conducted at  $20^\circ\text{C}$   
156 in 50 ml polypropylene centrifuge tubes containing a 0.01 M NaCl aqueous solution  
157 prepared with analytical grade NaCl.

158 To study Ga adsorption on calcite, 180 mL of a 0.01 M NaCl solution initially at  
159 equilibrium with the atmosphere was first allowed to equilibrate with 1g of calcite  
160 powder in a polypropylene bottle. The bottle with the suspension was kept sealed  
161 and continuously shaken for the following 24 hours in a thermostatic bath at  $20^\circ\text{C}$   
162 before adding any amount of HCl or NaOH to obtain the desired titration pH value.

163 After the addition of acid/base, the solution was allowed to equilibrate with the  
164 calcite powder for another 2-3 days while regularly measuring the pH, and adding  
165 supplementary amounts of acid or base if necessary, until a constant pH value was  
166 observed. Measurements of pH, Ca concentration and alkalinity after 2-3 days  
167 showed that the solution was in equilibrium with calcite. Each solution was  
168 subsequently filtered through a 0.22  $\mu\text{m}$  PTFE membranes into centrifuge tubes  
169 where a desired mass of calcite and fresh neutral Ga solution was then added  
170 successively. The centrifuge tubes were installed on a tube-rotator turning at a speed  
171 of about 20 rpm and mixed for at least 3 days. pH and Ca concentration measured at  
172 the end of the sorption runs were not found to change compared to their initial  
173 values. Ga adsorption onto the calcite surface was studied within the 7.4-8.6 pH  
174 range for different solid/aqueous solution ratios (3.6 - 40.3 g/l). The initial Ga  
175 concentration was fixed at 100 ppb, except for one experiment (C-11) in which the  
176 starting Ga concentration was 50 ppb.

177 For the batch adsorption experiments on goethite, the equilibration step between  
178 solution and sorbent was not necessary because of the very low solubility of  
179 goethite. In this case Ga was directly added to the goethite suspension without any  
180 preliminary processing. The initial Ga concentration varied between 0.1 and 58.6  
181 ppm for a solid/solution ratio ranging from 0.1 to 10.3 g/l and  $2.5 \leq \text{pH} \leq 10.5$ .  
182 Typical exposure time was about 1 week. We note that the Ga concentration of  
183 several experiments was above the predicted saturation with respect to  $\alpha\text{-GaOOH}$   
184 (cf. Bénézech et al., 1997). However, these concentrations were much lower than  
185 those used by Persson et al. (2006) to study Ga adsorption on goethite within the  
186 same pH range. These authors did not observe any formation of Ga precipitate from  
187 their solutions and showed that the measured changes in Ga concentration were the  
188 consequence of the strong adsorption of Ga on the goethite surface. At the end of  
189 the experiments, the aqueous solution from each experiment was sampled for  
190 chemical and isotopic analyses. The sampling was carried out with 10 ml  
191 polypropylene syringes by filtering the collected volume of solution with 0.22  $\mu\text{m}$   
192 PTFE filters. The filtrate was acidified with  $\text{HNO}_3$  and stored in a refrigerator until

193 analysis.

### 194 **2.3 pH measurements and chemical analyses**

195 The pH of the aqueous solution was carefully measured immediately after  
196 sampling on a non-filtered volume of the solution using a Metrohm pH  
197 microelectrode and a Metrohm 913 pH-meter with an accuracy of  $\pm 0.01$  units. Ca  
198 and Fe concentrations were measured by flame atomic absorption (AAS 400,  
199 Perkin-Elmer) with an uncertainty of  $\pm 1\%$  and a detection limit of 0.02 ppm,  
200 whereas Ga was analyzed by ICP-MS (Elan 6000, Perkin-Elmer) with an  
201 uncertainty less than 5% and a detection limit of 0.01 ppb.

### 202 **2.4 Ga isotope analyses**

203 Before isotopic analyses, Ga was purified from liquid samples using a two-stage  
204 ion exchange chromatography procedure on AG 1-X4 (Bio-rad) anion exchange  
205 resin and Ln spec (TrisKem) cation exchange resin using the protocol of Yuan et al.  
206 (2016). Briefly, prior to separation, acidified solutions ( $\text{HNO}_3$ ,  $\text{pH}\sim 1.5$ ) containing  
207 at least 200 ng of Ga were evaporated to dryness at  $100^\circ\text{C}$  on a hot plate and  
208 re-dissolved in  $\geq 1$  ml of 6 M HCl. Then, Ga was separated from other matrix  
209 elements using two chromatographic columns loaded with AG I-X4 and Ln-spec  
210 resin, respectively (see supporting information SI for the detailed description of the  
211 purification). Finally, the eluent containing only Ga recovered following separation  
212 of other elements was evaporated to dryness and the residual was dissolved in 2%  
213  $\text{HNO}_3$  for Ga isotope and concentration measurements on MC-ICP-MS and ICP-MS,  
214 respectively.

215 Most isotopic measurements were performed on a Neptune Plus MC-ICP-MS  
216 (Thermo Finnigan, Germany) at the Institute de Physique du Globe de Paris (IPGP,  
217 France), while a few were performed on a Nu Plasma MC-ICP-MS (Nu Instruments  
218 Ltd., UK) at the Institute of Geochemistry, Chinese Academy of Sciences (IGCAS,  
219 Guiyang, China). The MC-ICP-MS operating conditions are described in detail in  
220 Yuan et al. (2016) and summarized in the supporting information SI. Standards and  
221 samples were introduced by Ar flux into the plasma, with Ga concentrations of

222 about 20 µg/L and 50 µg/L in 2% HNO<sub>3</sub> for the Neptune Plus and Nu Plasma  
 223 MC-ICP-MS, respectively. In this study, the sample-standard bracketing (SSB)  
 224 method was employed to correct the mass bias for all measurements (e.g., Mason et  
 225 al., 2004). Ga isotope results were expressed as δ<sup>71</sup>Ga, in units of per mil (‰):

$$226 \quad \delta^{71}\text{Ga} = [({}^{71}\text{Ga}/{}^{69}\text{Ga})_{\text{sample}} / ({}^{71}\text{Ga}/{}^{69}\text{Ga})_{\text{NIST}} - 1] \times 1000 \quad (1)$$

227 where the subscript NIST defines the NIST SRM 994 Ga standard (Yang and Meija,  
 228 2010). The 2SD (standard deviations) of δ<sup>71</sup>Ga were calculated based on multiple  
 229 measurements of each solution and was generally lower than 0.05‰.

230 All isotopic measurements of this study were performed on the aqueous  
 231 solutions after filtration because of the much higher sensitivity of solutions to the  
 232 minor changes in isotopic composition compared to the bulk solid. Assuming that  
 233 the loss of Ga from the solution is solely accounted for by Ga adsorption on the  
 234 calcite or goethite surface and that the solids themselves are Ga-free, the isotope  
 235 ratio of adsorbed Ga (δ<sup>71</sup>Ga<sub>solid</sub>) can be calculated from the mass balance equation  
 236 using the isotope ratio in the aqueous phase (δ<sup>71</sup>Ga<sub>solution</sub>), the fraction of Ga  
 237 removed from the solution (*F*, % of initial amount), and the isotope ratio of the  
 238 initial solution used for the experiment (δ<sup>71</sup>Ga<sub>initial</sub>):

$$239 \quad \delta^{71}\text{Ga}_{\text{solid}} = [100 \times \delta^{71}\text{Ga}_{\text{initial}} - (100 - F) \times \delta^{71}\text{Ga}_{\text{solution}}] / F \quad (2)$$

240 A similar approach to calculate the isotopic composition of adsorbed elements  
 241 was used for Mo (Barling and Andbar, 2004), B (Lemarchand et al., 2005, 2007),  
 242 Cu and Zn (Balistreri et al., 2008), Si (Delstanche et al., 2009; Oelze et al., 2014),  
 243 and Ge (Pokrovsky et al., 2014). In using Eq. (2) we carefully verified the absence  
 244 of experimental artifacts due to sample handling and particularly filtration, which  
 245 could possibly invalidate the results of the calculation. It was found that filtration  
 246 did not change the δ<sup>71</sup>Ga value of the filtrate compared to the initial Ga stock  
 247 solution within the uncertainty of measurements (± 0.05‰, 2SD).

248 The difference in the isotopic composition of Ga adsorbed on the solid and Ga  
 249 in solution, Δ<sup>71</sup>Ga<sub>solid-solution</sub>, was calculated as:

$$250 \quad \Delta^{71}\text{Ga}_{\text{solid-solution}} = \delta^{71}\text{Ga}_{\text{solid}} - \delta^{71}\text{Ga}_{\text{solution}} \quad (3)$$

251 Note that if complete isotopic exchange between the solid and the solution occurs

252 during Ga adsorption on the solid surface (commonly referred as *closed system*  
253 *equilibrium*)  $\Delta^{71}\text{Ga}_{\text{solid-solution}}$  represents Ga equilibrium fractionation and is  
254 independent of the fraction  $F$  of Ga removed from the solution. In the case of  
255 irreversible Ga adsorption, on the contrary, adsorbed Ga does not continuously  
256 exchange with the solution and Rayleigh fractionation (Rayleigh, 1902) may best  
257 describe the change in  $\delta^{71}\text{Ga}_{\text{solution}}$  as a function of  $F$ .

258 The estimated uncertainties on the calculated  $\Delta^{71}\text{Ga}_{\text{solid-solution}}$  stem from i) the  
259 uncertainty on the calculated  $F$  value, and ii) the analytical uncertainty on the  
260 isotopic composition of the initial Ga solution and Ga isotopic ratio of each  
261 individual experiment.

## 262 **2.5 Thermodynamic calculations and Ga sorption modeling**

263 The distribution of species in solution and at the surface of calcite and goethite  
264 were modeled for each experiment using the code Visual MINTEQ v 3.1  
265 (Gustafsson, 2012). The activity coefficients of dissolved aqueous species were  
266 calculated using the Davies equation whereas the activity coefficients of surface  
267 species were assumed to be equal to 1. Dissolved inorganic carbon (DIC)  
268 concentrations and corresponding  $\text{CO}_2$  partial pressures ( $p\text{CO}_2$ ) for calcite  
269 adsorption experiments were obtained from measured pH's and Ca concentrations  
270 assuming thermodynamic equilibrium between aqueous solution and calcite. Ga  
271 aqueous speciation was calculated using the Ga hydrolysis constants reported by  
272 Benézéth et al. (1997), which were incorporated into the Visual MINTEQ  
273 thermodynamic database.

274 Ga adsorption on calcite was modeled using the surface complexation model  
275 established by Pokrovsky and Schott (2002), which builds on the detailed  
276 characterization of the calcite surface chemistry gained from the spectroscopic  
277 investigation and measurements of the charge and potential of the mineral/water  
278 interface (Van Cappelen et al., 1993; Pokrovsky et al., 1999; Pokrovky et al., 2000).  
279 According to this model, two primary hydration sites,  $>\text{CaOH}^0$  and  $>\text{CO}_3\text{H}^0$ , exist at  
280 the calcite surface, having a 1:1 stoichiometry. Successive

281 protonation/deprotonation of these sites and reactions with calcite constituent ions  
 282 ( $\text{Ca}^{2+}$  and  $\text{CO}_3^{2-}$ ) lead to the formation of the following surface  
 283 species:  $\text{>CaOH}_2^+$ ,  $\text{>CaO}^-$ ,  $\text{>CaHCO}_3^0$ ,  $\text{>CaCO}_3^-$ ,  $\text{>CO}_3^-$  and  $\text{>CO}_3\text{Ca}^+$ . The values  
 284 of the formation constants of these species, the electrical double-layer (EDL)  
 285 capacitance as well as the calcite surface site densities used in this study are listed in  
 286 Table 1. Ga was assumed to adsorb as a six-coordinated anion on single protonated  
 287 Ca-sites, in agreement with the X-ray absorption fine structure (XAFS)  
 288 characterization of local Ga structure at the calcite surface (Pokrovsky et al., 2004).  
 289 Expressed in terms of basis species of the thermodynamic database, Ga adsorption  
 290 at the calcite surface can be described as:



292 The determination of the intrinsic stability constant of reaction (4) was achieved by  
 293 a fitting procedure in which this constant was the only adjustable parameter, while  
 294 the constants of all other surface reactions, the EDL capacitance, and the densities  
 295 of surface sites were maintained constant (Table 1). An optimized value of the Ga  
 296 adsorption constant ( $K_4$ ) was obtained by sequential modeling of the experimental  
 297 results with PEST (Doherty, 2010).

298 The adsorption of Ga at the goethite surface was described by a 2-p*K* constant  
 299 capacitance model that has been adopted by many authors to describe the adsorption  
 300 of different aqueous species at the surface of this mineral (e.g. Lövgren et al., 1990;  
 301 Nilsson et al., 1992; Lumsdon and Evans, 1994; Pokrovsky et al., 2006). The values  
 302 of goethite surface acidity constants, taken from Lövgren et al. (1990), are reported  
 303 in Table 2 along with other parameters defining the surface complexation model  
 304 used in the present study. In agreement with the XAFS characterization of Ga  
 305 species adsorbed at the goethite surface and the surface complexation model of  
 306 Persson et al. (2006), we assumed that Ga formed a six-coordinated inner-sphere  
 307 mononuclear complex during the reaction of gallium with goethite surface  
 308 according to the following reaction involving the aqueous and surface basis species:



310 As for calcite, the constant value of reaction (5) was obtained by modeling our  
311 experimental results using Visual MINTEQ in combination with PEST. In this case,  
312 the density of goethite surface functional groups was fixed at  $1.68 \text{ nm}^{-2}$ , which  
313 corresponds to the density of hydroxyl groups experimentally determined by  
314 Lövgren et al. (1990), while the capacitance of the electric double layer was kept at  
315 the constant value of  $0.75 \text{ F/m}^2$ . These values are consistent with the site densities  
316 derived from crystallographic data (cf. Barrón and Torrent, 1996; Pivovarov, 1997)  
317 and the range of capacitance values commonly used for studying goethite surface  
318 complexation (Lumsdon and Evans, 1994; Cornell and Schwertmann, 2004).

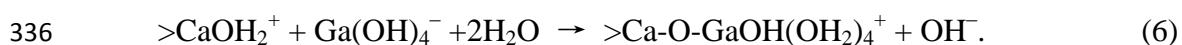
### 319 **3. RESULTS**

#### 320 **3.1 Ga adsorption and its modeling**

##### 321 *Calcite*

322 Ga adsorption results are listed in Table 3. It can be seen that the measured  
323 fraction of Ga adsorbed on calcite decreases with increasing pH, from 41.1 % at  
324 pH=7.5 to 9.5 % at pH=8.5. Table 3 also lists for each experiment the values of  
325 dissolved inorganic carbon (DIC) concentration and the corresponding  $\text{CO}_2$  partial  
326 pressures derived from measured pH and Ca concentration and the fraction of  
327 adsorbed Ga as calculated by modeling of the experimental data. The calculated  
328 fractions of Ga adsorbed were obtained for a best-fit  $\log K_4$  value of  $6.7 \pm 0.1$ , in  
329 good agreement with the estimates of Pokrovsky et al. (2004), who determined a  
330 value of  $7.0 \pm 0.3$  for the same reaction constant involving the basis species of the  
331 thermodynamic database.

332 Since in the range of investigated pH the dominant calcium surface species  
333 is  $>\text{CaOH}_2^+$  (cf. Pokrovsky et al. 2000), whereas  $\text{Ga}(\text{OH})_4^-$  dominates the Ga  
334 aqueous speciation (Bénézech et al., 1997), the adsorption of this element at the  
335 calcite/water interface can be expressed as:



337 The stability constant of reaction (6) can be deduced from the value of  $K_4$ , the Ga  
338 hydrolysis constants and the formation constant of  $>\text{CaOH}_2^+$  at the calcite surface

339 (see Table 1). Taking into account the values of these constants, the derived value of  
340  $\log K_6$  is equal to -3.49. A comparison between the experimental values of adsorbed  
341 Ga and those predicted by the surface complexation model using the determined  
342 value of  $K_4$  is provided in Fig. 1. It can be seen that a satisfactory agreement is  
343 obtained, the difference between measured and predicted values being of 8-12 % for  
344 4 samples but lower than 3% for all the others (see Table 3). In Fig. 2 the adsorbed  
345 Ga concentration (expressed in  $\text{nmol/m}^2$ ) was plotted against pH together with the  
346 predictions of the SCM model generated in this study for different  $p\text{CO}_2$  (three solid  
347 curves on the plot) and a calcite/solution ratio of 3.6 g/l. In one case (black solid  
348 line) the pH was varied by changing the  $\text{CO}_2$  partial pressure while maintaining the  
349 fluid at equilibrium with calcite. In contrast, the blue and red curves correspond to  
350 the model results obtained by fixing the  $p\text{CO}_2$  at  $1.0 \times 10^{-4}$  and  $1.5 \times 10^{-3}$  atm,  
351 respectively. These three curves represent plausible fit-lines to the experimental data  
352 within the relatively small range of experimental  $p\text{CO}_2$ , illustrating the good  
353 agreement between the data and the SCM model of Ga adsorption proposed here.

#### 354 *Goethite*

355 A summary of the experimental parameters and the corresponding results is  
356 reported in Table 4. Five of the runs were sampled a first time 3 days after Ga  
357 addition to the suspension (samples G-1, G-6, G-7, G-14 and G-20), and then after 7  
358 days as for all the other experiments. It can be observed that the difference in Ga  
359 adsorbed between 3 and 7 days is generally very small (0 - 2 %), suggesting that Ga  
360 reached adsorption equilibrium after time periods  $\leq 3$  days. The dependence of the  
361 fraction of adsorbed Ga on goethite concentration is illustrated in Fig. 3A. It can be  
362 seen that the extent of Ga adsorption is much weaker at  $\text{pH} = 2.5$  than at  $\text{pH} \geq 3.1$   
363 and less impacted by the increase of goethite concentration. At  $\text{pH} \geq 3.1$  the Ga  
364 adsorbed fraction (% Ga adsorbed) increased to 100 % when the goethite  
365 concentration reached 1 to 7 g/L, whereas the highest percentage of Ga adsorbed at  
366  $\text{pH} = 2.5$  was equal to 46 % relative to a goethite concentration of 10 g/L (Table 4).  
367 This observation is consistent with the results of Persson et al. (2006), who reported

368 100 % of Ga<sub>(aq)</sub> adsorbed on goethite at 3 < pH < 9.

369 The SCM we applied with the parameter values listed in Table 2 provided the  
370 best fit of the experimental data for Log  $K_5 = -1.05 \pm 0.2$ . The comparison between  
371 measured and calculated Ga adsorbed fractions reported in Table 4 shows that the  
372 model is in good agreement with the experimental results, with most of the  
373 calculated values differing by 0.1 - 10 % with respect to the experimental  
374 measurements. However, the difference between measured and calculated  
375 percentage of adsorbed Ga was higher for 6 experiments, varying between 11 and  
376 31 %. The measured percentage of Ga adsorbed at the goethite/aqueous solution  
377 interface is plotted as a function of pH in Fig. 3B and compared, for three different  
378 total Ga concentration values ( $[Ga]_{tot}$ ) representative of our experiments, with the  
379 percentage of adsorbed Ga calculated using reaction (5). Despite the variable Ga  
380 aqueous concentrations and the different goethite/solution ratios, it can be seen that  
381 the calculated curves conform to the experimental data well. The formation of the  
382 octahedral Ga surface complex  $[>FeOGa(OH)_2^0]$  could thus occur via the  
383 interaction with  $>FeOH_2^+$  sites of the dominant Ga aqueous species,  $Ga^{3+}$  at pH < 4  
384 and  $Ga(OH)_4^-$  at pH > 4.5, according to:



386 and



388 The values of the equilibrium constants of reactions (7) and (8) can be derived  
389 from the calculated value of the equilibrium constant of reaction (5), the protonation  
390 constant of goethite functional groups and the value of the fourth Ga hydrolysis  
391 constant adopted in this study (Benézéth et al., 1997). The Log  $K_7$  and Log  $K_8$  values  
392 thus calculated are equal to -8.52 and 7.14, respectively.

### 393 **3.2 Ga isotope fractionation during adsorption**

#### 394 *Calcite*

395 Our results listed in Table 5 show that in all experiments lighter Ga isotopes were

396 preferentially adsorbed onto the calcite surface, leaving experimental solutions  
397 isotopically heavier relative to the initial Ga stock solution ( $\delta^{71}\text{Ga}_{\text{initial}} = 1.83 \text{ ‰}$ ).  
398 The steady-state Ga isotopic composition of solutions was reached within 3 days  
399 since the 7-day replicates of the same runs resulted in almost identical Ga isotope  
400 compositions within errors.

401 The Ga isotopic composition of the solutions ( $\delta^{71}\text{Ga}_{\text{solution}}$ ) is plotted as a function  
402 of the fraction of Ga adsorbed on calcite in Fig 4A. It can be seen that  $\delta^{71}\text{Ga}_{\text{solution}}$   
403 did not exhibit significant variation with the solution pH in the investigated pH  
404 range (7.4 - 8.6). The data reported in Fig. 4B show that the extent of Ga isotope  
405 fractionation decreased slightly when the Ga fraction adsorbed on calcite increased,  
406 with  $\Delta^{71}\text{Ga}_{\text{calcite-solution}}$  decreasing from  $-0.97 \pm 0.21 \text{ ‰}$  to  $-1.27 \pm 0.63 \text{ ‰}$  when the  
407 fraction of Ga removed from solution decreased from  $\sim 40 \text{ ‰}$  to  $10 \text{ ‰}$ . Note,  
408 however, the large uncertainty affecting the  $-1.27 \text{ ‰}$  data due to the small extent of  
409 Ga adsorption.

#### 410 *Goethite*

411 The results of the 23 Ga sorption runs performed on goethite are summarized in  
412 Table 5 and illustrated by Fig. 5A and 5B where  $\delta^{71}\text{Ga}_{\text{solution}}$  and  $\Delta^{71}\text{Ga}_{\text{goethite-solution}}$ ,  
413 respectively, are plotted as a function of the fraction of adsorbed Ga. As for the  
414 sorption runs on calcite, the lighter Ga isotopes were preferentially adsorbed at the  
415 goethite surface, leaving the solutions isotopically heavier than the initial stock Ga  
416 solution ( $\delta^{71}\text{Ga}_{\text{initial}} = 1.87\text{‰}$ ). It should be noted that for the runs G-1, G-6, G-7,  
417 G-14 and G-20 performed at pH 2.5, 3.1, 3.1, 10.0 and 10.5, respectively, the fluid  
418 isotopic analyses relative to 3 and 7 days duration yielded the same results within  
419 errors (Table 5). Fig. 5A shows that  $\delta^{71}\text{Ga}_{\text{solution}}$  did not exhibit significant variation  
420 with solution pH in the large pH range investigated ( $2.5 \leq \text{pH} \leq 10.5$ ).

421 The extent of Ga isotope fractionation between goethite and solution ( $-0.89\text{‰} <$   
422  $\Delta^{71}\text{Ga}_{\text{goethite-solution}} < -0.45\text{‰}$ ) was distinctly smaller than that between calcite and  
423 solution ( $-1.27\text{‰} < \Delta^{71}\text{Ga}_{\text{calcite-solution}} < -0.97\text{‰}$ ) (Table 5 and Fig. 4B and 5B).  
424 Furthermore, Ga isotope fractionation between goethite and solution was impacted  
425 more than that between calcite and solution by the fraction of Ga adsorbed, the

426 extent of fractionation decreasing by  $\sim 0.2\%$  when the fraction of Ga removed from  
427 solution increased from 20% to near 100% (Fig. 5B).

## 428 **4. DISCUSSION**

### 429 **4.1 Ga isotope fractionation mechanisms**

430 The results of the experiments with both calcite and goethite are consistent with  
431 Ga isotope fractionation during adsorption onto the solid surfaces being the result of  
432 an equilibrium isotope effect. As seen in Figs 4A and 5A, the experimental  
433  $\delta^{71}\text{Ga}_{\text{solution}}$  and  $\delta^{71}\text{Ga}_{\text{solid}}$  data fall on single parallel linear trends and hence are best  
434 matched by closed system equilibrium exchange between dissolved and sorbed Ga.

435 Two main mechanisms could *a priori* account for the Ga isotope fractionations  
436 measured in this study: i) isotope exchange between Ga aqueous species and the Ga  
437 complexes formed at the solid surface, and ii) the preferential adsorption of a single  
438 type of Ga aqueous species if several Ga species of different isotopic composition  
439 co-exist in solution (i.e.  $\text{Ga}(\text{OH})_2^+$ ,  $\text{Ga}(\text{OH})_3^0$ ,  $\text{Ga}(\text{OH})_4^-$ ), which would  
440 subsequently shift the isotopic composition of the solution.

#### 441 *Calcite*

442 For this mineral, the preferential adsorption of a single type of Ga aqueous  
443 species can be ruled out because at the pH of our experimental solutions (7.4 - 8.6),  
444  $\text{Ga}(\text{OH})_4^-$  is the only Ga species present in solution (cf. Table 6 and Benézéth et al.,  
445 1997). Thus, the isotope exchange between  $\text{Ga}(\text{OH})_4^-$  and Ga surface complexes  
446 should be responsible for the isotope fractionation reported in the present study.

447 Ga sorption on calcite can be described by the interaction of  $\text{Ga}(\text{OH})_4^-$  with the  
448 hydrated surface calcium sites,  $>\text{CaOH}_2^+$ , leading to the formation of six-  
449 coordinated Ga surface anions,  $>\text{Ca-O-GaOH}(\text{OH}_2)_4^+$  sharing one oxygen with a Ca  
450 ion at the surface (reaction (6)). Aqueous Ga, therefore, changes its coordination  
451 from 4 to 6 when adsorbing on the calcite surface. XAFS observations showed that  
452 this coordination change results in an increase of the Ga-O bond length from  $1.84 \pm$   
453  $0.01 \text{ \AA}$  in  $\text{Ga}(\text{OH})_4^-$  (Pokrovski et al., 2002; Pokrovsky et al., 2004) to  $1.94 \pm 0.01 \text{ \AA}$   
454 in the Ga surface complexes (Pokrovsky et al., 2004). Given the general rule that at

455 equilibrium the heavy isotopes of an element would tend to concentrate in the  
456 species where that element forms the stiffest (shortest) bonds (Criss, 1999; Schauble,  
457 2004), aqueous  $\text{Ga}(\text{OH})_4^-$  should therefore be enriched in heavy isotopes ( $^{71}\text{Ga}$ )  
458 compared to the Ga surface complexes. This is exactly what we observed in all our  
459 experiments where Ga sorption on the calcite surface induces an enrichment of the  
460 solution in  $^{71}\text{Ga}$ .

461 The observed small decrease of the extent of Ga isotope fractionation with the  
462 increasing percentage of adsorbed Ga (Fig. 4B) might be related to the slight  
463 changes in the structure of Ga surface complexes with increasing degree of calcite  
464 surface coverage by adsorbed Ga. The XAFS study of Pokrovsky et al. (2004)  
465 indeed reported that adsorbed Ga at concentrations  $> 20 \text{ nmol/m}^2$  exhibited second  
466 shell contributions arising from Ga-Ga pairs with Ga-Ga distances ( $\sim 3.05$  and  $\sim 3.5$   
467  $\text{\AA}$ ) very similar to those observed by Pokrovski et al. (2002) for the polymeric Ga  
468 hydroxide complexes formed in aqueous solution during  $\text{Ga}^{3+}$  hydrolysis at  $2 < \text{pH}$   
469  $< 5$ . Since the mean of Ga-O distance in these polymers is distinctly shorter than  
470 that in the monomeric  $\text{Ga}(\text{H}_2\text{O})_{6-4}(\text{OH})_{0-2}$  species ( $1.88 \pm 0.03 \text{ \AA}$  vs  $1.96 \pm 0.01 \text{ \AA}$ ),  
471 it can be expected that the extent of isotope fractionation would be slightly reduced  
472 for the highest amount of Ga adsorbed at the calcite surface ( $\sim 10 \text{ nmol/m}^2$ ) which is  
473 indeed shown by our experimental data.

#### 474 *Goethite*

475 The striking feature of the results for goethite is that the solution pH had no  
476 discernable effect on the isotope fractionation, although Ga aqueous speciation  
477 dramatically differs at pH 2.5/3.1 (only hexacoordinated  $\text{Ga}^{3+}$  and  $\text{GaOH}^{2+}$ ) and pH  
478  $\geq 8$  (100%  $\text{Ga}(\text{OH})_4^-$ ) as shown in Table 6.

479 Ga adsorption modeling on goethite (this study; Persson et al., 2006) and the  
480 XAFS characterization of Ga local structure at the water-goethite interface (Persson  
481 et al., 2006) demonstrated the presence of octahedral Ga species,  $>\text{FeOGa}(\text{OH})_2^0$ ,  
482 sharing two edges and one corner with  $\text{FeO}_6$  octahedra at the goethite surface (see  
483 Fig. 6). If this surface complex was formed by the adsorption of octahedral aqueous  
484 Ga ( $\text{Ga}^{3+}/\text{Ga}(\text{OH})^{2+}$ ) and tetrahedral  $\text{Ga}(\text{OH})_4^-$  at  $\text{pH} \leq 3.1$  and  $\text{pH} \geq 8$ , respectively,

485 a greater extent of Ga isotope fractionation would be expected at  $\text{pH} \geq 8$  because of  
486 the Ga coordination (and Ga-O bond length) change between aqueous and sorbed  
487 gallium. The lack of effect of pH on Ga isotope fractionation likely indicates that Ga  
488 surface complexes are formed by the sorption of  $\text{Ga}(\text{OH})_4^-$  on the goethite surface at  
489 pH 2.5 and 3.1 as well as at  $\text{pH} \geq 8$ , although the proportion of  $\text{Ga}(\text{OH})_4^-$  in the bulk  
490 fluid is very small at  $\text{pH} \leq 3.1$  ( $< 0.5\%$  of total aqueous Ga). The preferential  
491 adsorption of  $\text{Ga}(\text{OH})_4^-$  at pH 2.5-3.1 likely results from i) the difficulty for  $\text{Ga}^{3+}$   
492 and  $\text{Ga}(\text{OH})^{2+}$  to get closer to the goethite surface because of the electrostatic  
493 repulsion generated by the  $>\text{FeOH}_2^+$  surface species which account for  $> 99\%$  of  
494 goethite surface speciation at  $\text{pH} \leq 3.1$ , and ii) by the increased hydroxide anion  
495 concentration in the Stern and diffusive layers near the solid surface due to proton  
496 loss by water molecules and anion diffusion to neutralize the goethite solution  
497 interface (Tamura et al., 2001; Hiemstra and Van Riemsdijk, 2006). The resulting  
498 increase of  $\text{OH}^-$  concentration (and thus pH) in the 0.1-1  $\mu\text{m}$  thick diffusive layer  
499 (Gupta et al., 2007) should favor  $\text{Ga}^{3+}$  hydrolysis and the formation of  $\text{Ga}(\text{OH})_4^-$ .  
500 For example, at  $\text{pH}=3$ , an increase in pH of the diffuse layer by only one unit would  
501 be enough to increase the proportion of  $\text{Ga}(\text{OH})_4^-$  from 0.01 to  $7\%^1$ . The change of  
502 Ga-O bond length between  $\text{Ga}(\text{OH})_4^-$  ( $\sim 1.84 \text{ \AA}$ ) and the surface complexes ( $\sim 1.96 \text{ \AA}$ )  
503 could thus explain the enrichment in lighter Ga isotope ( $^{69}\text{Ga}$ ) observed both at acid  
504 and alkaline pH on the surface of the solid.

505 The significant reduction of the extent of Ga isotope fractionation with the  
506 increasing fraction of Ga removed from solution may be related to the formation of  
507 Ga surface polymers with increasing degree of goethite surface coverage by Ga,  
508 similar to the case for calcite. The XAFS investigation of Ga local environment at  
509 the solution-goethite interface did not allow Persson et al. (2006) to detect second  
510 shell contributions arising from Ga-Ga pairs that characterize the presence of  
511 polymeric hydroxide complexes or  $\text{Ga}(\text{OH})_3$  surface precipitates. However, it  
512 should be noted that the fraction of goethite surface active sites occupied by Ga was

---

<sup>1</sup> Similarly, the borate anion,  $\text{B}(\text{OH})_4^-$ , has been shown to be selectively adsorbed on calcite surfaces to form tetrahedral surface complexes even at  $6.5 \leq \text{pH} \leq 7.7$  where this species account for only 0.17 to 2 % of total aqueous boron (Goldberg and Forster, 1991; Goldberg et al., 2000).

513  $\leq 29\%$  in Persson et al. (2006), whereas it ranged between 0.3 % (0.01  $\mu\text{mol}/\text{m}^2$ )  
514 and 180 % (5.04  $\mu\text{mol}/\text{m}^2$ ) in the present study. Therefore, it is likely that Ga  
515 surface polymers and/or  $\text{Ga}(\text{OH})_3$  surface precipitates were present for the highest  
516 Ga surface concentrations of this study (i.e.  $[\text{Ga}]_{\text{ads}} > 2 \mu\text{mol}/\text{m}^2$ ). Because the Ga-O  
517 bond lengths in monomeric  $>\text{FeOGa}(\text{OH})_2^0$  (1.96 Å) would be longer than in Ga  
518 surface polymers and  $\text{Ga}(\text{OH})_3(\text{s})$  ( $\sim 1.88$  Å), the latter should be enriched in  $^{71}\text{Ga}$ .  
519 This would explain the significant reduction of the extent of isotope fractionation  
520 observed in this study for the highest degree of Ga surface coverage ( $> 70\%$  of Ga  
521 removed from solution,  $[\text{Ga}]_{\text{ads}} > 2 \mu\text{mol}/\text{m}^2$ ).

## 522 **4.2 Geochemical applications**

523 The results obtained in this study allow for a first evaluation of the degree of Ga  
524 isotope fractionation in surficial environments where Ga-bearing solutions interact  
525 with calcium carbonates and/or Fe (oxyhydr)oxides. The fractionation factors  
526 measured in the present work imply that the infiltration of Ga-bearing fluids through  
527 soils or sediments containing carbonates and/or Fe (oxyhydr)oxides should induce  
528 enrichments of heavier Ga in the fluid up to 1.25‰ for low water/carbonate ratios or  
529 0.9‰ for low water/Fe (oxyhydr)oxide ratios, respectively. Though Ga isotope  
530 fractionation during its co-precipitation with Fe (oxyhydr)oxides has not been  
531 investigated at the present stage, comparable fractionation factors with enrichment  
532 of the liquid in heavier isotopes should occur during Ga coprecipitation with iron  
533 oxides because in these solids Ga substitutes for Fe in octahedral coordination  
534 (Martin et al., 1997). It is thus expected that rivers draining highly weathered  
535 magmatic rocks (i.e. in tropical or volcanic arc regions) will be enriched in  $^{71}\text{Ga}$  by  
536 about 1‰ relative to the unaltered bedrocks. Note that Rayleigh distillation may  
537 induce distinctly higher enrichment of heavy Ga in sediment pore waters during the  
538 progressive precipitation of Fe-oxides in marine or freshwater sediments, as  
539 observed for other isotope systems (i.e.  $\delta^{57}\text{Fe}$ , Rouxel et al., 2008). At the same time,  
540 when high amounts of organic matter are available in soils and rivers, the  
541 complexation of  $\text{Ga}(\text{OH})_4^-$  with carboxylic or hydroxyl-carboxylic acids, phenols,

542 di-phenols may lead to an enrichment of heavier Ga in free gallate ions, which is  
543 similar to the behavior of other metals (Fe, Cu, Zn, etc.) with organic ligands (Fujii  
544 et al., 2014), implying a potential application of Ga isotopes for tracing biological  
545 processes.

546 However, it should be noted that in most rivers with  $\text{pH} > 5$ , Ga, like Al, is not  
547 transported as a true dissolved ionic species but via organic, organo-mineral and  
548 mineral colloids or suspended species (e.g., Pokrovsky et al., 2010; Ogawa et al.,  
549 2012). Interestingly, as demonstrated by Pokrovsky et al. (2014) for boreal rivers, a  
550 significant fraction of Ga can be transferred to the true dissolved pool during  
551 estuarine mixing as a result of desorption from colloids and suspended species with  
552 progressive increase of pH to that of seawater. Thus, desorption processes in  
553 estuaries can lead to significant fluxes to the ocean of true dissolved Ga enriched in  
554  $^{71}\text{Ga}$ . On the other hand, according to Orians and Bruland (1998), most dissolved  
555 Ga at the surface of the oceans has, like Al, an eolian provenance with the extent of  
556 dissolution of Ga from eolian particles close to 50 %. Thus, as with estuarine  
557 mixing processes, reduction of Ga coordination accompanying this dissolution is  
558 likely to enrich the ocean in  $^{71}\text{Ga}$  as well as Ga scavenging by solid particles  
559 throughout the water column. Vertical profiles of dissolved Ga in the oceans (Orians  
560 and Bruland, 1988) show evidence, along with particle scavenging, of a deep water  
561 source of Ga from diffusion out of the sediments. This deep supply of dissolved Ga  
562 is also likely to be enriched in  $^{71}\text{Ga}$ . In the end, one could expect oceanic dissolved  
563 Ga to be isotopically heavier than Ga from the continental crust. Consequently, Ga  
564 isotopes would be a useful tool for tracing the impact of continental input (through  
565 both rivers and atmospheric deposition) on the oceanic biogeochemistry of Ga (and  
566 Al).

## 567 **5. CONCLUDING REMARKS**

568 In this study we carried out a series of experiments aimed at determining Ga  
569 isotope fractionation during Ga adsorption on calcite and goethite. Gallium  
570 adsorption and corresponding isotopic composition were investigated at 20 °C as a

571 function of pH and for different solid/solution ratios and initial aqueous Ga  
572 concentrations. Our results provide the first experimental evidence of significant Ga  
573 isotope fractionation during solid-fluid interactions. Adsorption of Ga on calcite and  
574 goethite surfaces results in substantial enrichments of the solid surfaces in light Ga  
575 isotopes with values of isotope fractionation factors,  $\Delta^{71}\text{Ga}_{\text{solid-solution}}$ , as great as  
576 -1.27‰ and -0.89‰ for calcite and goethite, respectively, indicating that Ga  
577 isotopes fractionate to a larger extent during adsorption on the surface of calcite  
578 than during adsorption on goethite. Our results suggest that the fractionation is  
579 mainly triggered by changes of Ga coordination and Ga-O bond length during  
580 adsorption of  $\text{Ga}(\text{OH})_4^-$  onto the solid surface.

581 Because Ga is present as tetrahedral gallate ions in most natural fluids and  
582 forms hexa-coordinated species at the surface of solids, it is likely that the  
583 adsorption of Ga by oxides, carbonates or clay minerals could yield significant Ga  
584 isotope fractionation between secondary minerals and surficial fluids including  
585 seawater. Our study demonstrates the potential of Ga isotopes to increase our  
586 understanding of biogeochemical processes at the Earth surface. However, further  
587 experimental and theoretical work is needed to quantify Ga isotope fractionation  
588 during Ga co-precipitation with secondary minerals (Fe/Mn hydroxides, Fe oxides,  
589 carbonates other than calcite, clays) and to further constrain the impact of fluid  
590 composition and pH on the extent of Ga isotope fractionation.

## 591 **ACKNOWLEDGMENTS**

592 Oleg S. Pokrovsky and Thomas D. Bullen are thanked for their helpful comments,  
593 constructive suggestions and careful English editing. This work was financially  
594 supported by the Natural Science Foundation of China (41625012, U1301231,  
595 41561134017, U1612442), the State Key Laboratory of Environmental  
596 Geochemistry, IGCAS (SKLEG2016001) and the GET Laboratory  
597 (CNRS-Toulouse University).

598  
599  
600

601 **REFERENCES**

- 602 Balistrieri, L.S., Borrok, D.M., Wanty, R.B., Ridley and W.I. (2008) Fractionation of Cu and  
603 Zn isotopes during adsorption onto amorphous Fe (III) oxyhydroxide: experimental  
604 mixing of acid rock drainage and ambient river water. *Geochim. Cosmochim. Acta* **72**,  
605 311-328.
- 606 Barling, J. and Anbar, A. (2004) Molybdenum isotope fractionation during adsorption by  
607 manganese oxides. *Earth Planet. Sc. Lett.* **217**, 315-329.
- 608 Barrón, V., and Torrent, J. (1996) Surface hydroxyl configuration of various crystal faces of  
609 hematite and goethite. *J. Colloid Interf. Sci.* **177**, 407-410.
- 610 Benézéth, P., Diakonov, I.I., Pokrovski, G.S., Dandurand, J.-L., Schott, J. and Khodakovsky,  
611 I.L. (1997) Gallium speciation in aqueous solution. Experimental study and modelling:  
612 Part 2. Solubility of  $\alpha$ -GaOOH in acidic solutions from 150 to 250 C and hydrolysis  
613 constants of gallium (III) to 300 C. *Geochim. Cosmochim. Acta* **61**, 1345-1357.
- 614 Berner, R. A. (1997) The rise of plants and their effect on weathering and atmospheric CO<sub>2</sub>.  
615 *Science* **276**, 544-546.
- 616 Burton, J., Culkin, F. and Riley, J. (1959) The abundances of gallium and germanium in  
617 terrestrial materials. *Geochim. Cosmochim. Acta* **16**, 151-180.
- 618 Cornell R. M. and Schwertmann U. (2004) The Iron Oxides: structures, properties,  
619 reactions, occurrences and uses. 2nd edition. Wiley-VCH. 670 p.
- 620 Criss, R.E. (1999) Principles of stable isotope distribution. Oxford University Press. 264 p.
- 621 De Laeter, J. R. (1972). The isotopic composition and elemental abundance of gallium in  
622 meteorites and in terrestrial samples. *Geochim. Cosmochim. Acta* **36**, 735-743.
- 623 Delstanche, S., Opfergelt, S., Cardinal, D., Elsass, F., André, L. and Delvaux, B. (2009)  
624 Silicon isotopic fractionation during adsorption of aqueous monosilicic acid onto iron  
625 oxide. *Geochim. Cosmochim. Acta* **73**, 923-934.
- 626 Doherty (2010). PEST. Model-independent parameter estimation. User Manual. 5th edition.  
627 Watermark Numerical Computing. Web: <http://www.pesthomepage.org>.
- 628 Fujii, T., Moynier, F., Blichert-Toft, J. and Albarède, F. (2014) Density functional theory  
629 estimation of isotope fractionation of Fe, Ni, Cu, and Zn among species relevant to  
630 geochemical and biological environments. *Geochim. Cosmochim. Acta* **140**, 553-576.
- 631 Gaillardet, J., Dupré, B., Louvat, P. and Allegre, C. (1999) Global silicate weathering and  
632 CO<sub>2</sub> consumption rates deduced from the chemistry of large rivers. *Chem. Geol.* **159**,  
633 3-30.
- 634 Gaillardet, J., Viers, J. and Dupré, B. (2003) Trace elements in river waters. *Treatise on*  
635 *geochemistry* 5, 225-272.
- 636 Galy, A. and France-Lanord, C. (1999) Weathering processes in the Ganges–Brahmaputra  
637 basin and the riverine alkalinity budget. *Chem. Geol.* **159**, 31-60.
- 638 Goldberg, S. and Forster, E.H. (1991) Boron sorption on calcareous soils and reference  
639 calcites. *Soil Sci.* **152**, 304-310.
- 640 Goldberg, S., Lesch, S.M., and Suarez, D.L. (2000) Predicting boron adsorption by soils  
641 using soil chemical parameters in the constant capacitance model. *Soil Sci. Soc. Am. J.*  
642 **64**, 1356-1363.
- 643 Goldschmidt, V.M. (1954) Geochemistry. LWW.
- 644 Gottardi, G., Burton, J. and Culkin, F. (1978) Gallium. *Handbook of geochemistry* 2, 3.

645 Gupta, A.K., Coelo, D., Adler, P.M. (2007) Influence of the Stern layer on elektokinetic  
646 phenomena in porous media. *J. Colloid Interf. Sci.* **316**, 140-159.

647 Gussone, N., Schmitt, A. D., Heuser, A., Wombacher, F., Dietzel, M., Tipper, E., and  
648 Schiller, M. (2016) Calcium stable isotope geochemistry. Springer Ed., 260 p.

649 Gustafsson J. P. (2012). Visual MINTEQ (v3.1). A Windows version of MINTEQA2.  
650 <http://vminteq.lwr.kth.se/>

651 Hiemstra, T. and Van Riemsdijk, W.H. (2006) On the relationship between charge  
652 distribution, surface hydration, and the structure of interface of metal hydroxides. *J.*  
653 *Colloid Interf. Sci.* **301**, 1-18.

654 Hilton, R.G., Galy, A., Hovius, N., Horng, M.-J. and Chen, H. (2011) Efficient transport of  
655 fossil organic carbon to the ocean by steep mountain rivers: An orogenic carbon  
656 sequestration mechanism. *Geology* **39**, 71-74.

657 Hindshaw, R. S., Reynolds, B. C., Wiederhold, J. G., Kretzschmar, R., and Bourdon, B.  
658 (2011) Calcium isotopes in a proglacial weathering environment: Damna glacier,  
659 Switzerland. *Geochim. Cosmochim. Acta* **75**, 106-118.

660 Hydes, D. (1979) Aluminum in seawater: Control by inorganic processes. *Science* **205**,  
661 1260-1262.

662 Hydes, D. (1983) Distribution of aluminium in waters of the North East Atlantic 25 N to 35  
663 N. *Geochim. Cosmochim. Acta* **47**, 967-973.

664 Hydes, D. and Liss, P. (1977) The behaviour of dissolved aluminium in estuarine and  
665 coastal waters. *Estuar. Coast. Mar. Sci.* **5**, 755-769.

666 Kato, C., Moynier, F., Foriel, J., Teng, F.-Z. and Puchtel, I.S. (2017) The gallium isotopic  
667 composition of the bulk silicate Earth. *Chem. Geol* **448**, 164-172.

668 Lemarchand, E., Schott, J. and Gaillardet, J. (2005) Boron isotopic fractionation related to  
669 boron sorption on humic acid and the structure of surface complexes formed. *Geochim.*  
670 *Cosmochim. Acta* **69**, 3519-3533.

671 Lemarchand, E., Schott, J. and Gaillardet, J. (2007) How surface complexes impact boron  
672 isotope fractionation: evidence from Fe and Mn oxides sorption experiments. *Earth*  
673 *Planet. Sc. Lett.* *Sc. Lett.* **260**, 277-296.

674 Lövgren, L., Sjöberg, S. and Schindler, P.W. (1990) Acid/base reactions and Al (III)  
675 complexation at the surface of goethite. *Geochim. Cosmochim. Acta* **54**, 1301-1306.

676 Lumsdon, D.O. and Evans, L.J. (1994) Surface complexation model parameters for goethite  
677 ( $\alpha$ -FeOOH). *J. Colloid Interf. Sci.* **164**, 119-125.

678 Martell, A.E. and Hancock, R.D. (2013) Metal complexes in aqueous solutions. *Springer*  
679 *Science & Business Media*.

680 Martin, F., Ildefonse, P., Hazemann, J., Mathe, P., Noack, Y., Grauby, O., Beziat, D. and De  
681 Parseval, P. (1997) Gallium crystal chemistry in synthetic goethites. *Le Journal de*  
682 *Physique IV* **7**, C2-821-C822-822.

683 Mason, T.F., Weiss, D.J., Horstwood, M., Parrish, R.R., Russell, S.S., Mullane, E. and Coles,  
684 B.J. (2004) High-precision Cu and Zn isotope analysis by plasma source mass  
685 spectrometry Part 2. Correcting for mass discrimination effects. *J. Anal. Atom.*  
686 *Spectrom.* **19**, 218-226.

687 Measures, C. and Edmond, J. (1988) Aluminium as a tracer of the deep outflow from the  
688 Mediterranean. *J. Geophys. Res-Oceans* **93**, 591-595.

689 Nilsson, N., Lövgren, L. and Sjöberg, S. (1992) Phosphate complexation at the surface of  
690 goethite. *Chem. Spec. Bioavailab.* **4**, 121-130.

691 Oelze, M., von Blanckenburg, F., Hoellen, D., Dietzel, M. and Bouchez, J. (2014) Si stable  
692 isotope fractionation during adsorption and the competition between kinetic and  
693 equilibrium isotope fractionation: Implications for weathering systems. *Chem. Geol*  
694 **380**, 161-171.

695 Ogawa, Y., Ishiyama, D., Shikazono, N., Iwane, K., Kajiwara, M. and Tsuchiya, N. (2012)  
696 The role of hydrous ferric oxide precipitation in the fractionation of arsenic, gallium,  
697 and indium during the neutralization of acidic hot spring water by river water in the  
698 Tama River watershed, Japan. *Geochim. Cosmochim. Acta* **86**, 367-383.

699 Opfergelt, S., Georg, R. B., Delvaux, B., Cabidoche, Y. M., Burton, K. W., and Halliday, A.  
700 N. (2012) Mechanisms of magnesium isotope fractionation in volcanic soil weathering  
701 sequences, Guadeloupe. *Earth Planet. Sc. Lett.* **341**, 176-185.

702 Orians, K.J. and Bruland, K.W. (1988) The marine geochemistry of dissolved gallium: a  
703 comparison with dissolved aluminum. *Geochim. Cosmochim. Acta* **52**, 2955-2962.

704 Pearson, R. (1963) Soft and hard acids and bases. *J. Am. Chem. Soc.* **12**, 3538-3546.

705 Persson, P., Zivkovic, K. and Sjöberg, S. (2006) Quantitative adsorption and local structures  
706 of Gallium (III) at the water-alpha-FeOOH interface. *Langmuir* **22**, 2096-2104.

707 Pivovarov, S. (1997) Surface structure and site density of the oxide-solution interface. *J.*  
708 *Colloid Interf. Sci.* **196**, 321-323.

709 Pokrovski, G.S., Schott, J., Hazemann, J.-L., Farges, F. and Pokrovsky, O.S. (2002) An  
710 X-ray absorption fine structure and nuclear magnetic resonance spectroscopy study of  
711 gallium-silica complexes in aqueous solution. *Geochim. Cosmochim. Acta* **66**,  
712 4203-4222.

713 Pokrovsky, O.S. and Schott, J. (2002) Surface chemistry and dissolution kinetics of divalent  
714 metal carbonates. *Environ. Sci. Technol.* **36**, 426-432.

715 Pokrovsky, O.S., Schott, J., and Thomas, F. (1999) Processes at the magnesium-bearing  
716 carbonate/solution interface. 1. A surface speciation model of magnesite. *Geochim.*  
717 *Cosmochim. Acta* **63**, 863-880.

718 Pokrovsky, O.S., Pokrovski, G. and Schott, J. (2004) Gallium (III) adsorption on carbonates  
719 and oxides: X-ray absorption fine structure spectroscopy study and surface  
720 complexation modeling. *J. Colloid Interf. Sci.* **279**, 314-325.

721 Pokrovsky, O.S., Pokrovski, G., Schott, J. and Galy, A. (2006) Experimental study of  
722 germanium adsorption on goethite and germanium coprecipitation with iron hydroxide:  
723 X-ray absorption fine structure and macroscopic characterization. *Geochim.*  
724 *Cosmochim. Acta* **70**, 3325-3341.

725 Pokrovsky O.S., Mielczarski J. A., Barres O. and Schott J. (2000) Surface speciation  
726 models of calcite and dolomite/aqueous solution interfaces and their  
727 spectroscopic evaluation. *Langmuir* **16**, 2677-2688.

728 Pokrovsky, O.S., Viers, J., Shirokova, L., Shevchenko, V., Filipov, A. and Dupré, B. (2010)  
729 Dissolved, suspended, and colloidal fluxes of organic carbon, major and trace elements  
730 in the Severnaya Dvina River and its tributary. *Chem. Geol* **273**, 136-149.

731 Pokrovsky, O.S., Galy, A., Schott, J., Pokrovski, G.S. and Mantoura, S. (2014) Germanium  
732 isotope fractionation during Ge adsorption on goethite and its coprecipitation with Fe

oxy (hydr) oxides. *Geochim. Cosmochim. Acta* **131**, 138-149.

Rayleigh, L. (1902) On the distillation of binary mixtures. *Phil. Mag.* **S. 6 4**, 521-537.

Rouxel, O., Sholkovitz, E., Charette, M. and Edwards, K.J. (2008) Iron isotope fractionation in subterranean estuaries. *Geochim. Cosmochim. Acta* **72**, 3413-3430.

Schauble, E.A. (2004) Applying stable isotope fractionation theory to new systems. *Rev. Mineral. Geochem.* **55**, 65-111.

Schott, J., Mavromatis, V., Fujii, T., Pearce, C.R. and Oelkers, E.H. (2016) The control of carbonate mineral Mg isotope composition by aqueous speciation: Theoretical and experimental modeling. *Chem. Geol.* **445**, 120-134.

Shiller, A.M. (1988) Enrichment of dissolved gallium relative to aluminum in natural waters. *Geochim. Cosmochim. Acta* **52**, 1879-1882.

Shiller, A.M. and Frilot, D.M. (1996) The geochemistry of gallium relative to aluminum in Californian streams. *Geochim. Cosmochim. Acta* **60**, 1323-1328.

Tagirov, B. and Schott, J. (2001) Aluminum speciation in crustal fluids revisited. *Geochim. Cosmochim. Acta* **65**, 3965-3992.

Tamura, H., Mita, K., Tanaka, A., Makoto, I. (2001) Mechanism of hydroxylation of metal oxide surfaces. *J. Colloid Interf. Sci.* **243**, 202-207.

Teng, F. Z., Li, W. Y., Rudnick, R. L., and Gardner, L. R. (2010) Contrasting lithium and magnesium isotope fractionation during continental weathering. *Earth Planet. Sc. Lett.* **300**, 63-71.

Tipper, E.T., Bickle, M.J., Galy, A., West, A.J., Pomiès, C. and Chapman, H.J. (2006) The short term climatic sensitivity of carbonate and silicate weathering fluxes: insight from seasonal variations in river chemistry. *Geochim. Cosmochim. Acta* **70**, 2737-2754.

Van Cappellen, P., Charlet, L., Stumm, W, and Wersin, P. (1993) A surface speciation model of the carbonate mineral-aqueous solution interface. *Geochim. Cosmochim. Acta* **57**, 3505-3518.

Vance, D., Teagle, D.A. and Foster, G.L. (2009) Variable Quaternary chemical weathering fluxes and imbalances in marine geochemical budgets. *Nature* **458**, 493-496.

Wedepohl, K.H. (1995) The composition of the continental crust. *Geochim. Cosmochim. Acta* **59**, 1217-1232.

Wood, S.A. and Samson, I.M. (2006) The aqueous geochemistry of gallium, germanium, indium and scandium. *Ore Geol. Rev.* **28**, 57-102.

Yang, L. and Meija, J. (2010) Resolving the germanium atomic weight disparity using multicollector ICPMS. *Anal. Chem.* **82**, 4188-4193.

Yuan, W., Chen, J.B., Birck, J.-L., Yin, Z.Y., Yuan, S.L., Cai, H.M., Wang, Z.W., Huang, Q. and Wang, Z.H. (2016) Precise Analysis of Gallium Isotopic Composition by MC-ICP-MS. *Anal. Chem.* **88**, 9606-9613.

Zhang, T., Zhou, L., Yang, L., Wang, Q., Feng, L.-p. and Liu, Y.-s. (2016) High precision measurements of gallium isotopic compositions in geological materials by MC-ICP-MS. *J. Anal. Atom. Spectrom.* **31**, 1673-1679.

1 **Table 1.** Surface complexation reactions describing Ga adsorption on calcite with the  
 2 corresponding intrinsic stability constants taken from Pokrovsky and Schott (2002)  
 3 (reactions 1–6) and determined in this study (reactions 7–8). The values of the other  
 4 parameters defining the SCM of our system are as follows: EDL capacitance = 17  
 5 F/m<sup>2</sup>; surface site density= 8.22 μmol/m<sup>2</sup>.

| Surface reaction   | log $K_{int}^0$ (25 °C, $I=0$ ) |
|--|---------------------------------|
| 1. $>CO_3H^0 = >CO_3^- + H^+$                              | -5.1                            |
| 2. $>CO_3H^0 + Ca^{2+} = >CO_3Ca^+ + H^+$                  | -1.7                            |
| 3. $>CaOH^0 = >CaO^- + H^+$                                | -12.0                           |
| 4. $>CaOH^0 + H^+ = CaOH_2^+$                              | 11.85                           |
| 5. $>CaOH^0 + CO_3^{2-} + 2H^+ = >CaHCO_3^0 + H_2O$        | 23.50                           |
| 6. $>CaOH^0 + CO_3^{2-} + H^+ = >CaCO_3^- + H_2O$          | 17.1                            |
| 7. $>CaOH^0 + Ga^{3+} + 5H_2O = Ca-H_9GaO_6^+ + 2H^+$      | 6.70 ± 0.1                      |
| 8. $>CaOH_2^+ + Ga(OH)_4^- + 2H_2O = Ca-H_9GaO_6^+ + OH^-$ | -3.49                           |

6

7 **Table 2.** Surface complexation reactions used to model Ga adsorption on goethite.  
 8 Intrinsic goethite surface acidity constants (reactions 1 & 2) are taken from Lövgren et  
 9 al. (1990) whereas the intrinsic constants of formation of the Ga-complex (reactions  
 10 3-5) were determined in this study. EDL capacitance = 0.75 F/m<sup>2</sup>; surface site  
 11 density= 1.68 nm<sup>-2</sup> (2.79 μmol/m<sup>2</sup>).

| Goethite Surface reactions  | $\log K_{int}^0(25\text{ }^\circ\text{C. } I=0)$ |
|---|--|
| 1. $>\text{FeOH}^0 + \text{H}^+ = >\text{FeOH}_2^+$   | 7.47   |
| 2. $>\text{FeOH}^0 = >\text{FeO}^- + \text{H}^+$  | -9.51  |
| 3. $>\text{FeOH}^0 + \text{Ga}^{3+} + 2\text{H}_2\text{O} = >\text{FeOGa}(\text{OH})_2^0 + 3\text{H}^+$             | -1.05 ± 0.2                                      |
| 4. $>\text{FeOH}_2^+ + \text{Ga}^{3+} + 2\text{H}_2\text{O} \rightarrow >\text{FeOGa}(\text{OH})_2^0 + 4\text{H}^+$ | -8.52  |
| 5. $>\text{FeOH}_2^+ + \text{Ga}(\text{OH})_4^- \rightarrow >\text{FeOGa}(\text{OH})_2^0 + 2\text{H}_2\text{O}$     | 7.14   |

12

13 **Table 3.** Summary of the Ga adsorption experiments on calcite with the  
 14 corresponding pH, solid to aqueous solution ratios (Cc/Vol) and the relative  
 15 concentrations of Ca, dissolved inorganic carbon (DIC) and calculated  $p\text{CO}_2$ . All  
 16 experiments were conducted at the constant electrolyte (NaCl) concentration of 0.01  
 17 M. Note that total dissolved carbon and corresponding  $p\text{CO}_2$  were calculated on the  
 18 basis of measured Ca concentrations and pH's assuming thermodynamic equilibrium  
 19 with calcite. The table also lists the Ga aqueous concentration measured before and  
 20 after each experiment, the surface density of Ga adsorbed, and the comparison  
 21 between measured and modeled percentage of Ga adsorbed (last two columns).

| Sample No.  | pH  | Cc/Vol | [Ca] | DIC  | log $p\text{CO}_2$ | [Ga] <sub>in</sub> | [Ga] <sub>fin</sub> | [Ga] <sub>tot</sub> | [Ga] <sub>ads</sub> | % Ga adsorbed |      |
|-------------|-----|--------|------|------|--------------------|--------------------|---------------------|---------------------|---------------------|---------------|------|
|             |     |        |      |      |                    |                    |                     |                     |                     | g/l           | mM   |
| <b>C-1</b>  | 7.4 | 3.6    | 3.13 | 1.84 | -2.41              | 107.5              | 80.1                | 22.8                | 5.8                 | 25.5          | 25.8 |
| <b>C-2</b>  | 7.4 | 3.6    | 3.03 | 1.90 | -2.40              | 107.5              | 79.9                | 22.7                | 5.8                 | 25.7          | 25.8 |
| <b>C-3</b>  | 7.5 | 3.6    | 3.58 | 1.29 | -2.67              | 106.7              | 74.4                | 22.9                | 6.9                 | 30.3          | 22.0 |
| <b>C-4</b>  | 7.5 | 3.7    | 2.79 | 1.60 | -2.57              | 103.3              | 68.2                | 21.8                | 7.4                 | 34.0          | 22.1 |
| <b>C-5</b>  | 7.5 | 8.1    | 3.28 | 1.39 | -2.63              | 106.6              | 62.8                | 10.2                | 4.2                 | 41.1          | 38.6 |
| <b>C-6</b>  | 8.0 | 6.7    | 1.24 | 1.01 | -3.24              | 105.3              | 88.3                | 12.1                | 1.9                 | 16.1          | 13.3 |
| <b>C-7</b>  | 8.1 | 25.1   | 0.98 | 1.01 | -3.34              | 105.7              | 81.6                | 3.2                 | 0.7                 | 22.8          | 31.0 |
| <b>C-8</b>  | 8.2 | 40.2   | 0.83 | 0.93 | -3.47              | 106.5              | 78.6                | 2.0                 | 0.5                 | 26.2          | 36.0 |
| <b>C-9</b>  | 8.5 | 10.1   | 0.68 | 0.57 | -3.99              | 105.6              | 95.6                | 8.1                 | 0.8                 | 9.5           | 6.5  |
| <b>C-10</b> | 8.6 | 40.1   | 0.48 | 0.63 | -4.04              | 106.4              | 90.0                | 2.0                 | 0.3                 | 15.4          | 17.5 |
| <b>C-11</b> | 8.6 | 40.3   | 0.51 | 0.61 | -4.06              | 53.4               | 44.8                | 1.0                 | 0.2                 | 16.1          | 17.6 |

22

23

24 **Table 4.** Summary of the Ga adsorption experiments on goethite with the  
 25 corresponding pH, solid to aqueous solution ratios (Gth/Vol) and initial and final  
 26 concentration of Ga in solution. Total and adsorbed Ga amounts ( $[Ga]_{tot}$  and  $[Ga]_{ads}$ )  
 27 are expressed in terms of the goethite surface area [ $\mu\text{mol}/\text{m}^2$ ] of each experiment. The  
 28 last 2 columns list the adsorbed Ga percentage measured and calculated according to  
 29 the surface complexation model presented in this study.

| Sample No.   | pH   | Gth/Vol<br>g/l | $[Ga]_{in}$<br>ppm | $[Ga]_{fin}$<br>ppm | $[Ga]_{tot}$<br>$\mu\text{mol}/\text{m}^2$ | $[Ga]_{ads}$<br>$\mu\text{mol}/\text{m}^2$ | % Ga adsorbed |       |
|--------------|------|----------------|--------------------|---------------------|--|--|---------------|-------|
|              |      |                |                    |                     |  |  | measured      | Model |
| <b>G-1*</b>  | 2.5  | 9.9            | 55.383             | 30.253              | 3.45                                       | 1.57                                       | 45.4          | 45.7  |
| <b>G-1b</b>  | 2.5  | 9.9            | 55.383             | 29.905              | 3.45                                       | 1.59                                       | 46.0          | 46.0  |
| <b>G-2</b>   | 2.5  | 5.1            | 58.644             | 42.154              | 7.12                                       | 2.00                                       | 28.1          | 24.2  |
| <b>G-3</b>   | 2.5  | 4.1            | 58.517             | 44.394              | 8.81                                       | 2.13                                       | 24.1          | 19.7  |
| <b>G-4</b>   | 2.5  | 3.0            | 5.414              | 3.772               | 1.13                                       | 0.34                                       | 30.3          | 61.4  |
| <b>G-5</b>   | 2.5  | 2.0            | 5.054              | 3.745               | 1.53                                       | 0.40                                       | 25.9          | 52.5  |
| <b>G-6*</b>  | 3.1  | 9.7            | 53.571             | 1.264               | 3.40                                       | 3.32                                       | 97.6          | 92.7  |
| <b>G-6b</b>  | 3.1  | 9.7            | 53.571             | 1.266               | 3.40                                       | 3.32                                       | 97.6          | 92.7  |
| <b>G-7*</b>  | 3.1  | 4.9            | 52.071             | 13.515              | 6.62                                       | 4.90                                       | 74.0          | 56.6  |
| <b>G-7b</b>  | 3.1  | 4.9            | 52.071             | 12.417              | 6.62                                       | 5.04                                       | 76.2          | 58.5  |
| <b>G-8</b>   | 8.0  | 1.0            | 0.101              | 0.000               | 0.06                                       | 0.06                                       | 100.0         | 99.5  |
| <b>G-9</b>   | 8.0  | 6.9            | 0.103              | 0.000               | 0.01                                       | 0.01                                       | 100.0         | 99.9  |
| <b>G-10</b>  | 8.9  | 1.0            | 0.605              | 0.001               | 0.36                                       | 0.36                                       | 99.8          | 96.3  |
| <b>G-11</b>  | 9.0  | 0.5            | 0.604              | 0.007               | 0.70                                       | 0.69                                       | 98.9          | 91.3  |
| <b>G-12</b>  | 9.0  | 0.2            | 0.609              | 0.096               | 1.72                                       | 1.45                                       | 84.2          | 80.1  |
| <b>G-13</b>  | 9.5  | 0.5            | 1.247              | 0.278               | 1.45                                       | 1.12                                       | 77.7          | 74.6  |
| <b>G-14*</b> | 10.0 | 10.3           | 4.790              | 0.057               | 0.29                                       | 0.28                                       | 98.8          | 95.3  |
| <b>G-14b</b> | 10.0 | 10.3           | 4.790              | 0.044               | 0.29                                       | 0.28                                       | 99.1          | 95.3  |
| <b>G-15</b>  | 10.0 | 2.0            | 4.959              | 1.098               | 1.52                                       | 1.18                                       | 77.9          | 76.9  |
| <b>G-16</b>  | 10.0 | 1.0            | 4.985              | 3.005               | 2.99                                       | 1.19                                       | 39.7          | 53.7  |
| <b>G-17</b>  | 10.0 | 0.5            | 4.921              | 3.969               | 5.94                                       | 1.15                                       | 19.3          | 29.3  |
| <b>G-18</b>  | 10.0 | 0.2            | 5.176              | 4.086               | 17.05                                      | 3.59                                       | 21.1          | 11.5  |
| <b>G-19</b>  | 10.1 | 0.1            | 5.262              | 4.492               | 22.94                                      | 3.36                                       | 14.6          | 7.8   |
| <b>G-20*</b> | 10.5 | 10.3           | 4.960              | 0.842               | 0.30                                       | 0.25                                       | 83.0          | 84.6  |
| <b>G-20b</b> | 10.5 | 10.3           | 4.960              | 0.803               | 0.30                                       | 0.25                                       | 83.8          | 84.7  |
| <b>G-21</b>  | 10.5 | 1.0            | 4.962              | 3.805               | 3.00                                       | 0.70                                       | 23.3          | 28.6  |
| <b>G-22</b>  | 10.5 | 2.0            | 4.970              | 2.340               | 1.51                                       | 0.80                                       | 52.9          | 48.6  |
| <b>G-23</b>  | 10.5 | 4.0            | 4.971              | 1.046               | 0.77                                       | 0.61                                       | 79.0          | 67.5  |

30 \* This symbol identifies data relative to 3 days of adsorption reaction.

32 **Table 5.** Results of Ga isotope fractionation during adsorption on calcite and goethite. The  
 33 uncertainty of all isotopic measurements (expressed as 2 standard deviation, 2SD) are relative  
 34 to the 3 replicate measurements carried out for each sample. The isotopic composition of the  
 35 initial Ga (III) nitrate hydrate ( $\delta^{71}\text{Ga}_{\text{initial}}$ ) was of 1.83‰ and 1.87‰ for the adsorption  
 36 experiments conducted with calcite and goethite, respectively.

| Adsorbent       | Sample No.              | Exposure Time (days) | pH   | Ga adsorbed % | $\delta^{71}\text{Ga}_{\text{solution}} \pm 2\text{SD} (\text{‰})$ | $\delta^{71}\text{Ga}_{\text{solid}} \pm 2\text{SD} (\text{‰})$ | $\Delta^{71}\text{Ga}_{\text{solid-solution}} \pm 2\text{SD} (\text{‰})$ |
|-----------------|-------------------------|----------------------|------|---------------|--|---|--|
| <i>Calcite</i>  |                         |                      |      |               |  |   |  |
|                 | <b>C-1</b>              | 7                    | 7.4  | 25.5          | 2.10 ± 0.05  | 1.04 ± 0.02   | -1.06 ± 0.22   |
|                 | <b>C-2</b>              | 7                    | 7.4  | 25.7          | 2.08 ± 0.05  | 1.11 ± 0.02   | -0.97 ± 0.21   |
|                 | <b>C-3</b>              | 7                    | 7.5  | 30.3          | 2.19 ± 0.06  | 1.00 ± 0.02   | -1.19 ± 0.20   |
|                 | <b>C-4</b>              | 7                    | 7.5  | 34.0          | 2.18 ± 0.06  | 1.15 ± 0.01   | -1.03 ± 0.17   |
|                 | <b>C-5</b>              | 7                    | 7.5  | 41.1          | 2.25 ± 0.04  | 1.23 ± 0.01   | -1.02 ± 0.12   |
|                 | <b>C-6</b>              | 7                    | 8.0  | 16.1          | 2.02 ± 0.05  | 0.84 ± 0.06   | -1.18 ± 0.36   |
|                 | <b>C-7</b>              | 7                    | 8.1  | 22.8          | 2.09 ± 0.05  | 0.95 ± 0.03   | -1.14 ± 0.24   |
|                 | <b>C-8</b>              | 7                    | 8.2  | 26.2          | 2.10 ± 0.05  | 1.07 ± 0.02   | -1.03 ± 0.22   |
|                 | <b>C-9</b>              | 7                    | 8.5  | 9.5           | 1.95 ± 0.05  | 0.68 ± 0.16   | -1.27 ± 0.63   |
|                 | <b>C-10</b>             | 7                    | 8.6  | 15.4          | 2.01 ± 0.04  | 0.84 ± 0.06   | -1.17 ± 0.33   |
|                 | <b>C-11</b>             | 7                    | 8.6  | 16.1          | 2.02 ± 0.05  | 0.84 ± 0.06   | -1.18 ± 0.39   |
| <i>Goethite</i> |                         |                      |      |               |  |   |  |
|                 | <b>G-1*</b>             | 3                    | 2.5  | 45.4          | 2.22 ± 0.04  | 1.44 ± 0.10   | -0.78 ± 0.11   |
|                 | <b>G-1b</b>             | 7                    | 2.5  | 46.0          | 2.18 ± 0.04  | 1.50 ± 0.10   | -0.68 ± 0.11   |
|                 | <b>G-2</b>              | 7                    | 2.5  | 28.1          | 2.08 ± 0.05  | 1.34 ± 0.19   | -0.73 ± 0.20   |
|                 | <b>G-3</b>              | 7                    | 2.5  | 24.1          | 2.04 ± 0.03  | 1.34 ± 0.20   | -0.70 ± 0.20   |
|                 | <b>G-4</b>              | 7                    | 2.5  | 30.3          | 2.11 ± 0.05  | 1.32 ± 0.17   | -0.80 ± 0.18   |
|                 | <b>G-5</b>              | 7                    | 2.5  | 25.9          | 2.11 ± 0.04  | 1.47 ± 0.13   | -0.64 ± 0.13   |
|                 | <b>G-6*</b>             | 3                    | 3.1  | 97.6          | 2.37 ± 0.03  | 1.86 ± 0.04   | -0.52 ± 0.05   |
|                 | <b>G-6b</b>             | 7                    | 3.1  | 97.6          | 2.37 ± 0.05  | 1.86 ± 0.04   | -0.52 ± 0.07   |
|                 | <b>G-7*</b>             | 3                    | 3.1  | 74.0          | 2.30 ± 0.05  | 1.72 ± 0.06   | -0.58 ± 0.07   |
|                 | <b>G-7b</b>             | 7                    | 3.1  | 76.2          | 2.31 ± 0.04  | 1.73 ± 0.06   | -0.58 ± 0.07   |
|                 | <b>G-12</b>             | 7                    | 9.0  | 84.2          | 2.31 ± 0.03  | 1.79 ± 0.05   | -0.53 ± 0.06   |
|                 | <b>G-13</b>             | 7                    | 9.5  | 77.7          | 2.29 ± 0.05  | 1.75 ± 0.05   | -0.55 ± 0.07   |
|                 | <b>G-14*</b>            | 3                    | 10.0 | 98.8          | 2.36 ± 0.03  | 1.86 ± 0.04   | -0.49 ± 0.05   |
|                 | <b>G-14b</b>            | 7                    | 10.0 | 99.1          | 2.39 ± 0.04  | 1.87 ± 0.04   | -0.52 ± 0.06   |
|                 | <b>G-15</b>             | 3                    | 10.0 | 77.9          | 2.30 ± 0.04  | 1.75 ± 0.05   | -0.56 ± 0.07   |
|                 | <b>G-16</b>             | 7                    | 10.0 | 39.7          | 2.16 ± 0.04  | 1.42 ± 0.12   | -0.74 ± 0.13   |
|                 | <b>G-17</b>             | 7                    | 10.0 | 19.3          | 2.04 ± 0.04  | 1.16 ± 0.28   | -0.89 ± 0.28   |
|                 | <b>G-18</b>             | 7                    | 10.0 | 21.1          | 2.02 ± 0.05  | 1.30 ± 0.26   | -0.73 ± 0.26   |
|                 | <b>G-19<sup>†</sup></b> | 7                    | 10.1 | 14.6          | 1.94 ± 0.05  | 1.48 ± 0.40   | -0.45 ± 0.40   |
|                 | <b>G-20*</b>            | 3                    | 10.5 | 83.0          | 2.33 ± 0.03  | 1.78 ± 0.05   | -0.56 ± 0.06   |
|                 | <b>G-20b</b>            | 7                    | 10.5 | 83.8          | 2.34 ± 0.02  | 1.78 ± 0.05   | -0.56 ± 0.05   |
|                 | <b>G-21</b>             | 3                    | 10.5 | 23.3          | 2.04 ± 0.05  | 1.31 ± 0.23   | -0.72 ± 0.23   |

|             |   |      |      |                 |                 |                  |
|-------------|---|------|------|-----------------|-----------------|------------------|
| <b>G-22</b> | 7 | 10.5 | 52.9 | $2.25 \pm 0.05$ | $1.53 \pm 0.09$ | $-0.72 \pm 0.10$ |
| <b>G-23</b> | 7 | 10.5 | 79.0 | $2.33 \pm 0.05$ | $1.75 \pm 0.05$ | $-0.59 \pm 0.07$ |

---

37 \* This symbol identifies data relative to 3 days of adsorption reaction.

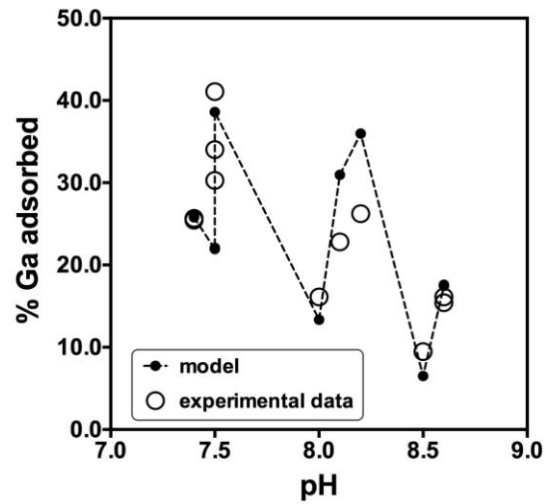
38 † datapoint not reported in Fig.5B because of the big uncertainty related to the small adsorption extent.

39

40 **Table 6.** Distribution of Ga aqueous species as a function of pH at 25°C (Bénézeth et  
 41 al., 1997; Persson et al., 2006).

| pH   | Distribution of Ga aqueous species at 25°C (I = 0.01, NaCl)                              |   |
|------|--|---|
|      | <i>Bénézeth et al. (1997)</i>  | <i>Persson et al. (2006)</i>  |
| 2.5  | 81% Ga <sup>3+</sup> , 19% Ga(OH) <sup>2+</sup>  | 95% Ga <sup>3+</sup> , 5% Ga(OH) <sup>2+</sup>                              |
| 3.1  | 48% Ga <sup>3+</sup> , 50% Ga(OH) <sup>2+</sup> ,<br>2% Ga(OH) <sub>2</sub> <sup>+</sup> | 49% Ga <sup>3+</sup> , 49% Ga(OH) <sub>3</sub> ,<br>2% Ga(OH) <sup>2+</sup> |
| ≥8.0 | 100% Ga(OH) <sub>4</sub> <sup>-</sup>  | 100% Ga(OH) <sub>4</sub> <sup>-</sup>                                       |

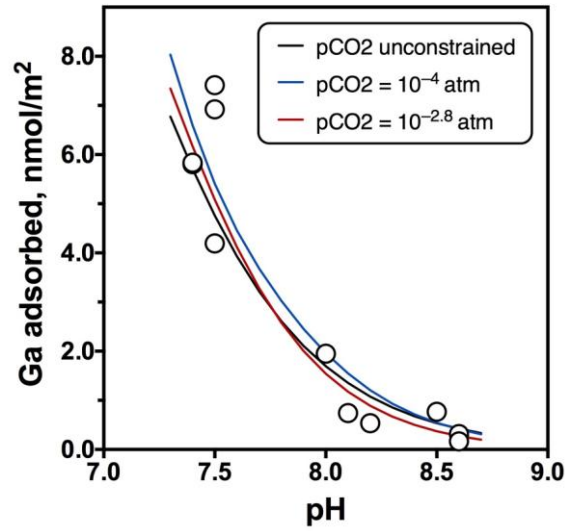
42



1

2 **Figure 1.** Comparison between the measured percentages of adsorbed Ga on calcite  
3 (empty circles) and those predicted by the SCM (black dots connected by the dashed  
4 line). Note that the experiments were conducted with solid/fluid ratios varying  
5 between 3.6 and 40.3 g/l. Initial Ga concentrations were of 100 ppb except for run  
6 C-11 ( $Ga_0=50$  ppb; cf. Table 3).

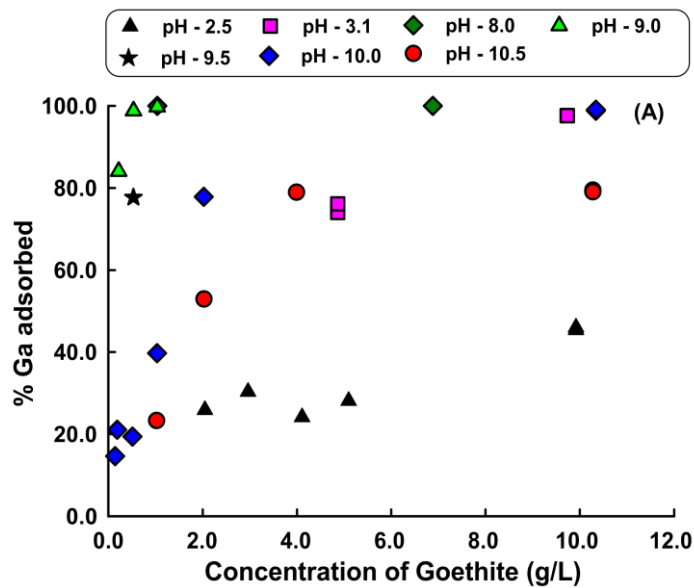
7



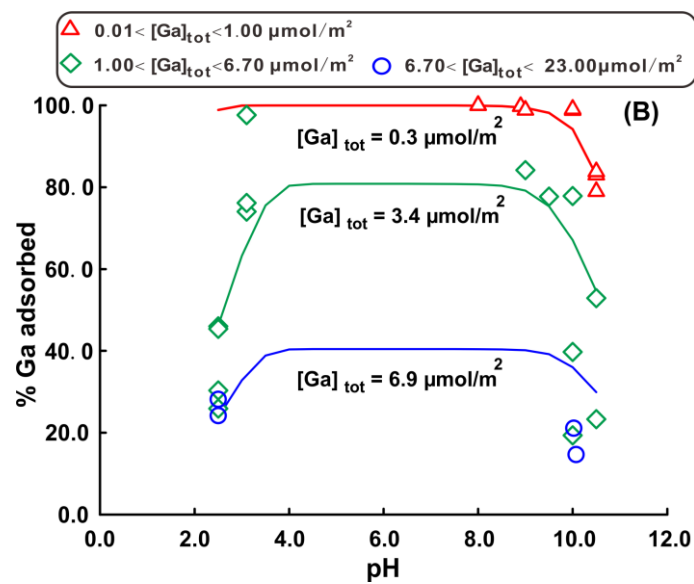
8 **Figure 2.** Measured Ga adsorption on calcite surface as a function of pH (symbols)  
 9 and SCM predictions (solid lines) for different values of  $p\text{CO}_2$ . The black line is  
 10 obtained by changing the  $\text{CO}_2$  partial pressure ( $5.6 \times 10^{-5} < p\text{CO}_2 < 7.3 \times 10^{-3}$  atm),  
 11 whereas blue and red lines were obtained by fixing  $p\text{CO}_2$  at  $1.0 \times 10^{-4}$  and  $1.5 \times 10^{-3}$   
 12 atm, respectively.

13

14



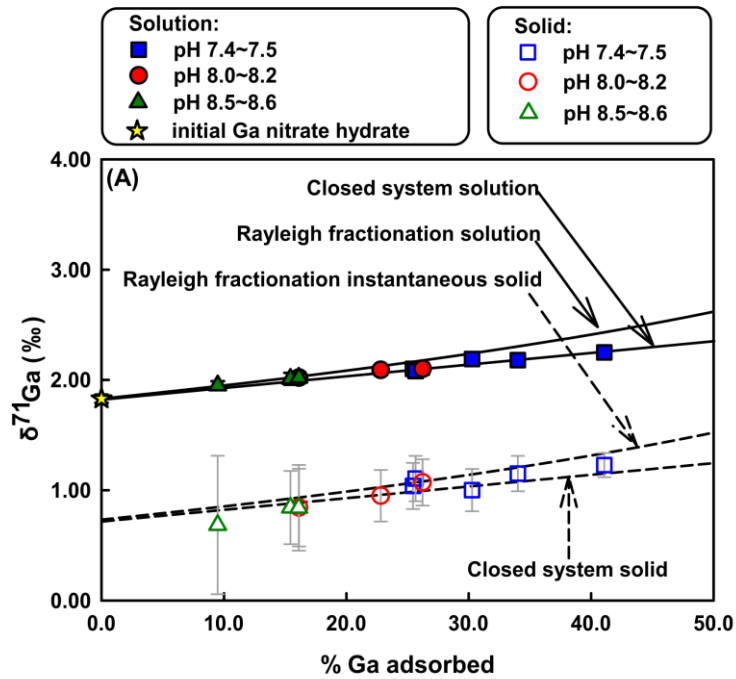
15



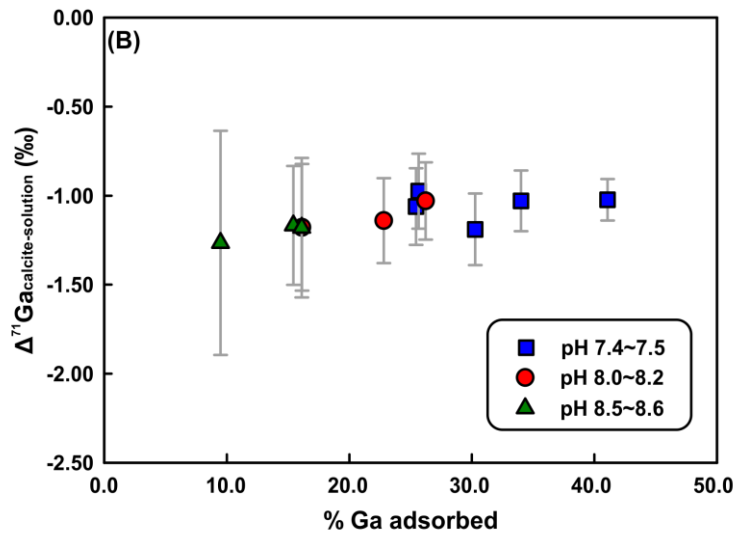
16

17 **Figure 3.** Percentage of Ga adsorbed as a function of goethite/aqueous solution  
18 volume ratio (A) and comparison between measured and calculated percentages of  
19 adsorbed Ga as a function of pH in 0.01 M NaCl (B). The three curves shown in  
20 Fig.3B represent the predictions of the SCM presented in this study for three  
21 different values of surface normalized total Ga concentration ( $[Ga]_{tot} = 0.3, 3.4$  and  
22  $6.9 \mu\text{mol}/\text{m}^2$ ), which are representative of our experiments (see Table 4).

23



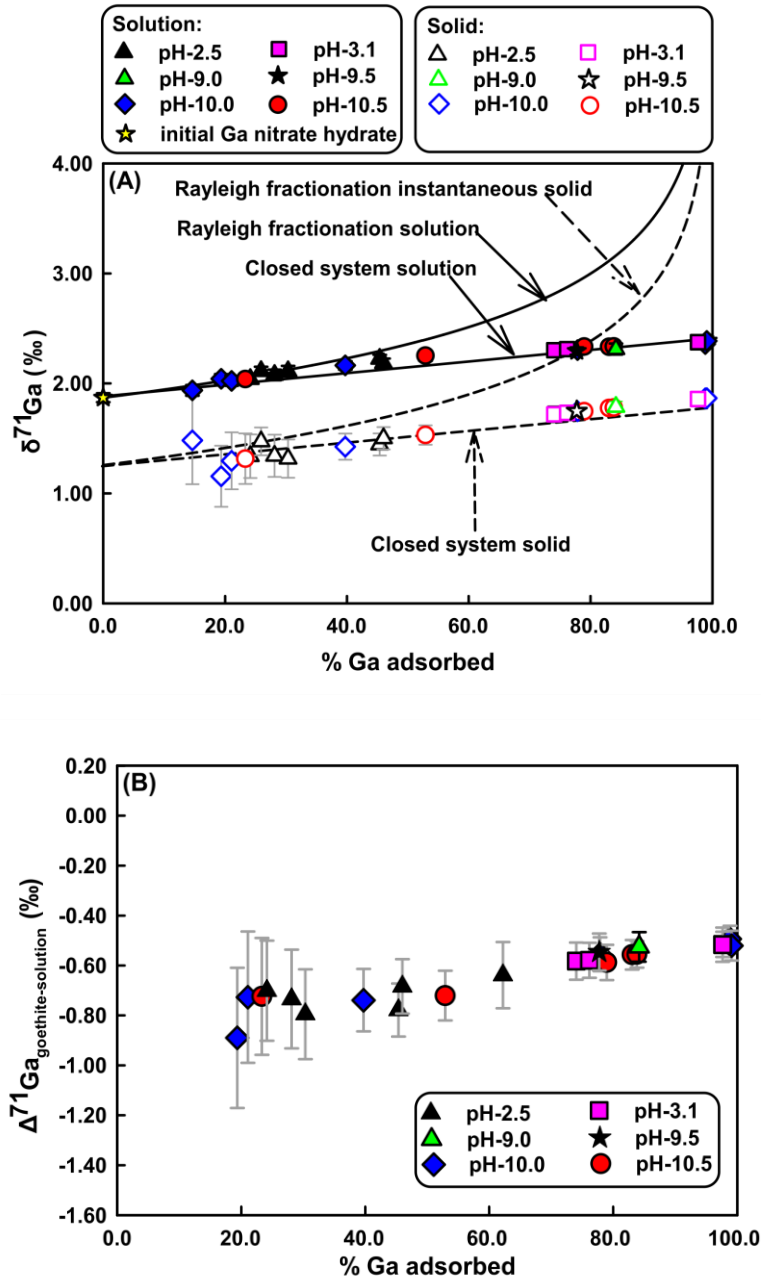
24



25

26 **Figure 4.**  $\delta^{71}\text{Ga}_{\text{solution}}$  and  $\delta^{71}\text{Ga}_{\text{calcite}}$  (both measured and inferred) as a function of the  
 27 fraction of Ga adsorbed by calcite (A), and the extent of Ga isotope fractionation  
 28 during Ga sorption on calcite ( $\Delta^{71}\text{Ga}_{\text{calcite-solution}}$ ) vs. the fraction of Ga adsorbed (B).  
 29 In (A) the experimental data are compared with the trends predicted for closed system  
 30 equilibrium and Rayleigh fractionation models calculated using  $\alpha_{\text{calcite-solution}} = 0.9989$   
 31 (runs C-1, C-3, C-7).  
 32

33



34

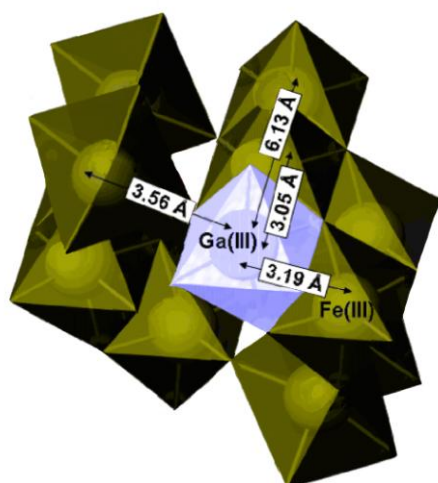
35 **Figure 5.**  $\delta^{71}\text{Ga}_{\text{solution}}$  and  $\delta^{71}\text{Ga}_{\text{goethite}}$  (both measured and inferred) as a function of the  
 36 fraction of Ga adsorbed by goethite (A), and the extent of Ga isotope fractionation  
 37 during Ga sorption on goethite ( $\Delta^{71}\text{Ga}_{\text{goethite-solution}}$ ) vs. the fraction of Ga adsorbed (B).  
 38 In (A) the experimental data are compared with the trends predicted for closed system  
 39 equilibrium and Rayleigh fractionation models calculated using  $\alpha_{\text{goethite-solution}} = 0.9993$   
 40 (runs G-1, G-1b, G-16, G-22).

41

42

43

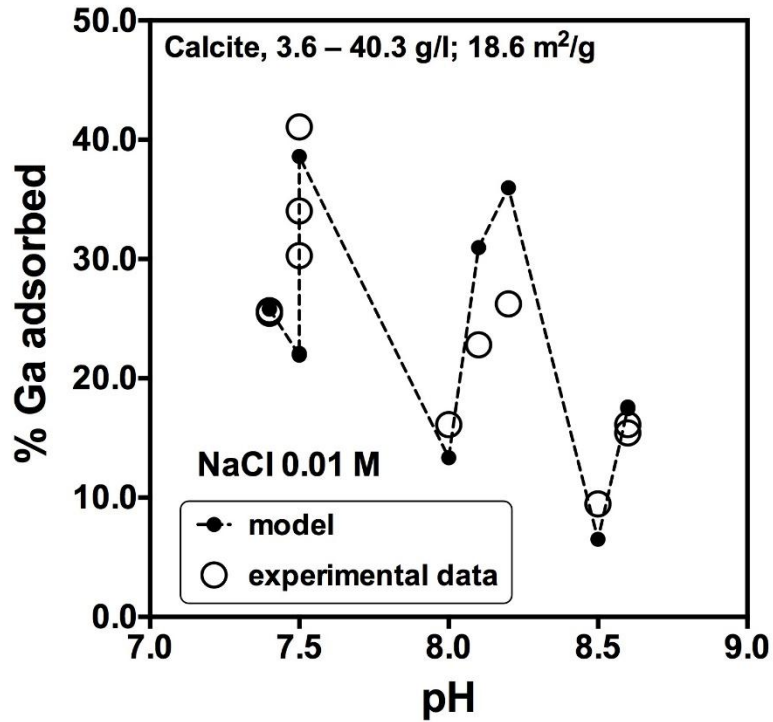
44



45

46

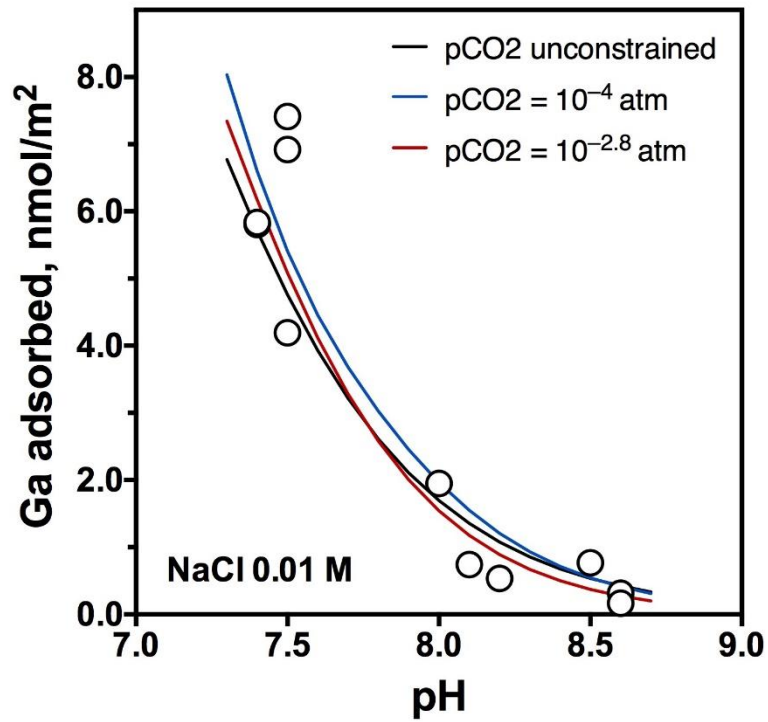
47 **Figure 6.** Schematic structure of the atomic environment of Ga(III) adsorbed onto  
48 goethite surface based on EXAFS spectroscopy (modified from Persson et al., 2006).



1

2 **Figure 1.** Comparison between the measured percentages of adsorbed Ga on calcite  
 3 (empty circles) and those predicted by the SCM (black dots connected by the dashed  
 4 line). Note that the experiments were conducted with different solid/fluid ratios. Initial  
 5 Ga concentrations were of 100 ppb except for run C-11 ( $Ga_0=50$  ppb; cf. Table 3).

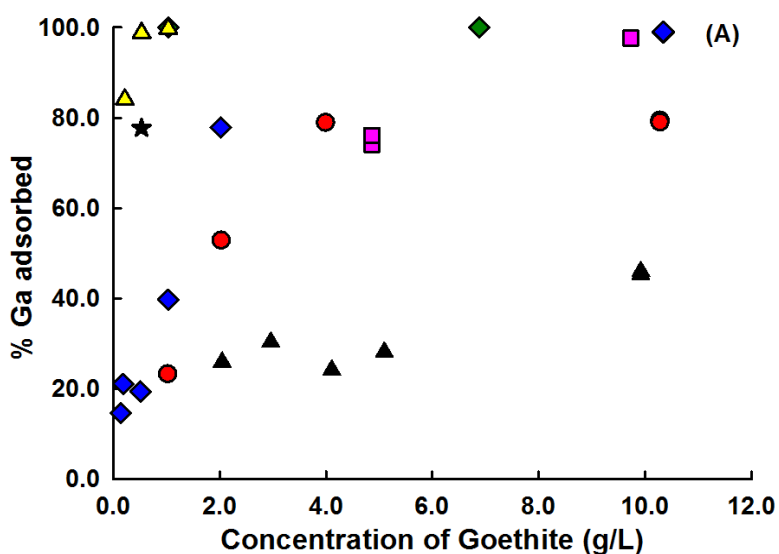
6



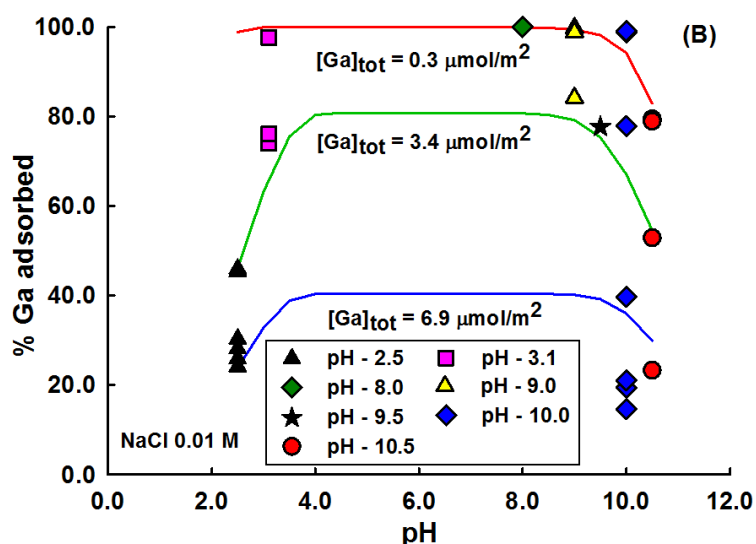
7

8 **Figure 2.** Measured Ga adsorption on calcite surface as a function of pH (symbols) and  
 9 SCM predictions (solid lines) for different values of  $p\text{CO}_2$ . The black line is obtained  
 10 by changing the  $\text{CO}_2$  partial pressure ( $5.6 \times 10^{-5} < p\text{CO}_2 < 7.3 \times 10^{-3}$  atm), whereas blue  
 11 and red lines were obtained by fixing  $p\text{CO}_2$  at  $1.0 \times 10^{-4}$  and  $1.5 \times 10^{-3}$  atm, respectively.

12



13

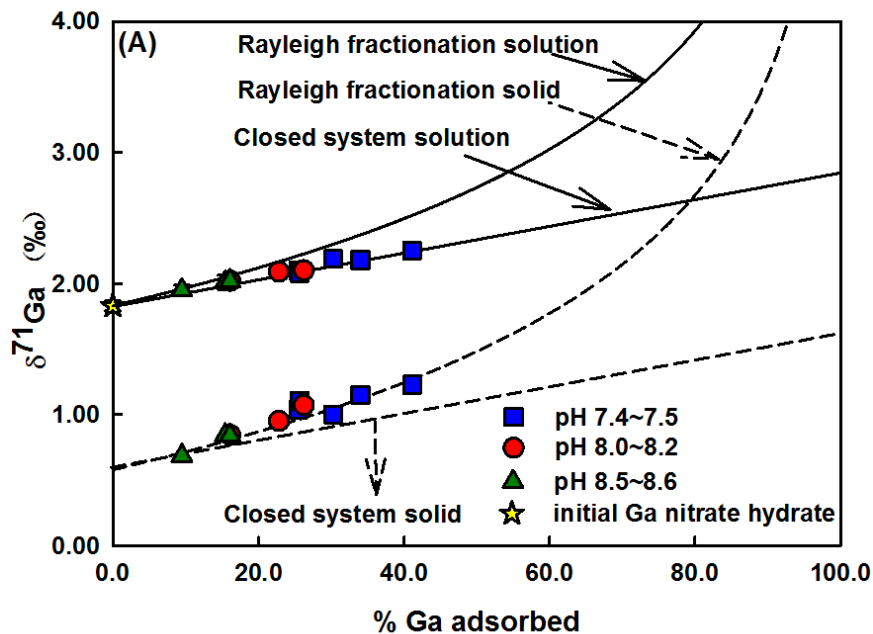


14

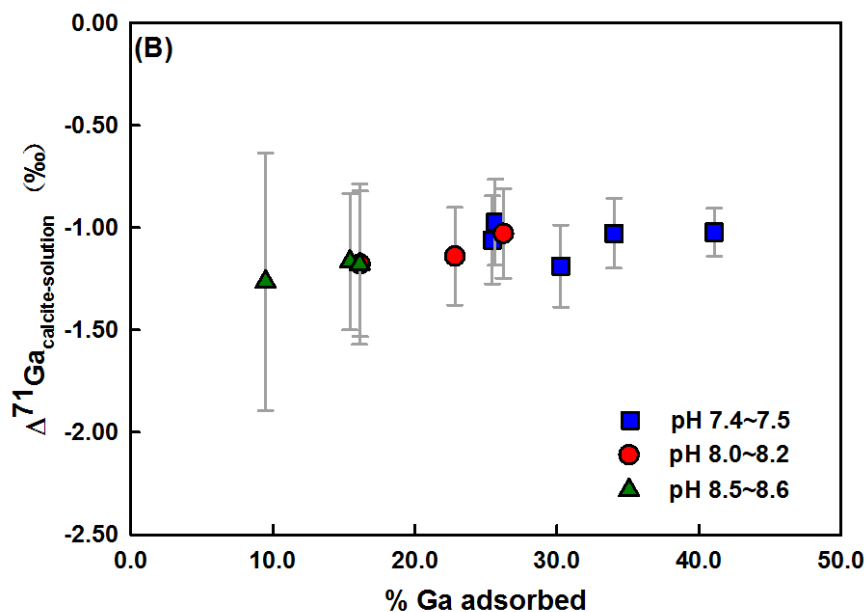
15 **Figure 3.** Percentage of Ga adsorbed as a function of goethite/aqueous solution  
16 volume ratio (A) and comparison between measured and calculated percentages of  
17 adsorbed Ga as a function of pH (B). The three curves drawn on the plot area of (B)  
18 represent the predictions of the SCM presented in this study for three different values  
19 of surface normalized total Ga concentration ( $[Ga]_{tot} = 0.3, 3.4$  and  $6.9 \mu\text{mol/m}^2$ ),  
20 which are representative of our experiments (see Table 4).

21

22  
23



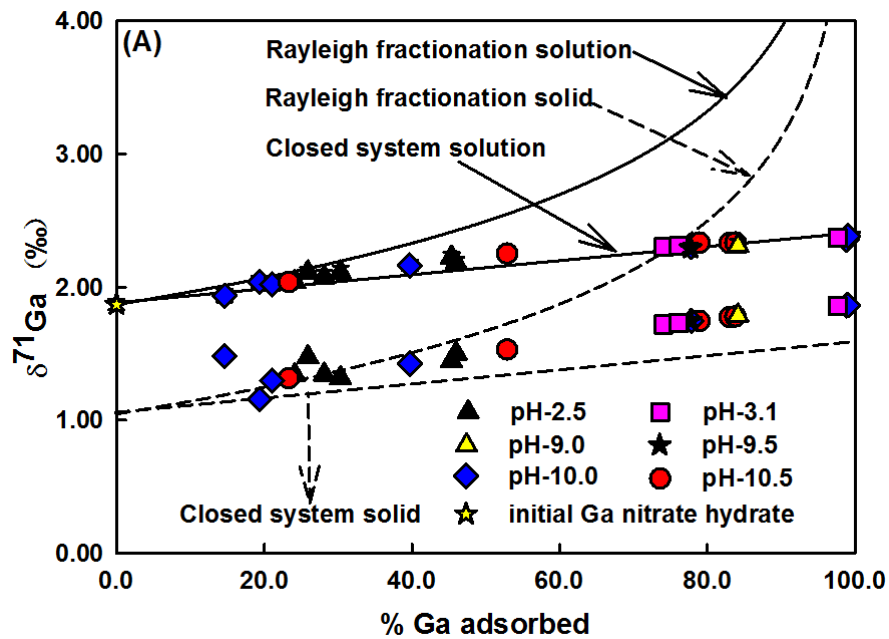
24  
25



26  
27  
28  
29  
30  
31  
32  
33

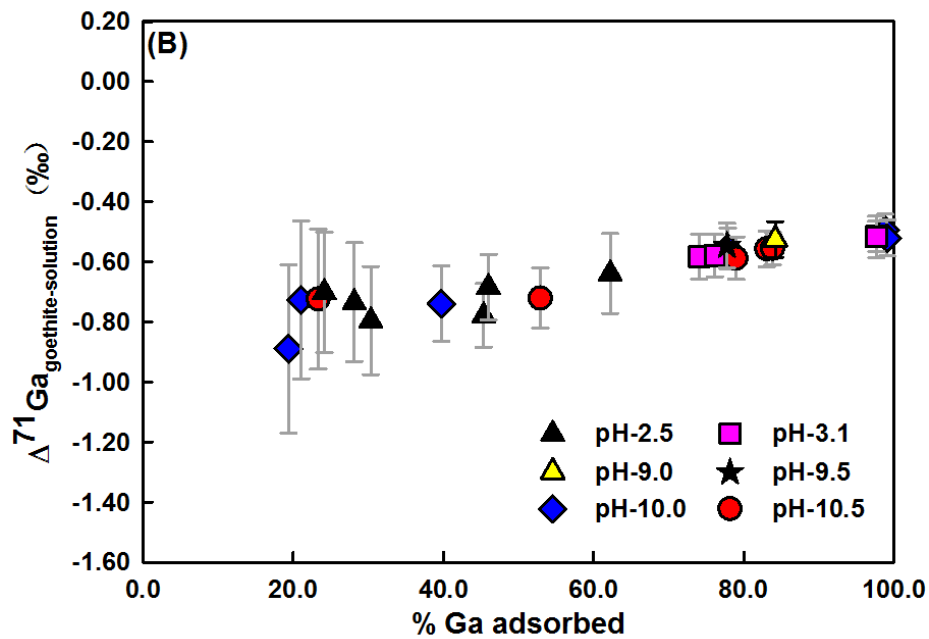
**Figure 4.**  $\delta^{71}\text{Ga}_{\text{solution}}$  and  $\delta^{71}\text{Ga}_{\text{calcite}}$  (both measured and inferred) as a function of the fraction of Ga adsorbed by calcite (A), and the extent of Ga isotope fractionation during Ga sorption on calcite ( $\Delta^{71}\text{Ga}_{\text{calcite-solution}}$ ) vs the fraction of Ga adsorbed (B). In (A) the experimental data are compared with the trends predicted for closed system equilibrium and Rayleigh fractionation models calculated using  $\alpha_{\text{calcite-solution}} = 0.9987$  (run C-9).

34



35

36



37

38

39 **Figure 5.**  $\delta^{71}\text{Ga}_{\text{solution}}$  and  $\delta^{71}\text{Ga}_{\text{goethite}}$  (both measured and inferred) as a function of the  
 40 fraction of Ga adsorbed by goethite (A), and the extent of Ga isotope fractionation  
 41 during Ga sorption on goethite ( $\Delta^{71}\text{Ga}_{\text{goethite-solution}}$ ) vs the fraction of Ga adsorbed (B).  
 42 In (A) the experimental data are compared with the trends predicted for closed system  
 43 equilibrium and Rayleigh fractionation models calculated using  $\alpha_{\text{goethite-solution}} = 0.9991$   
 44 (run G-17).  
 45

**Appendix**

[Click here to download Appendix: 4-Supporting Information\\_rev\\_final.doc](#)